JGR Oceans

RESEARCH ARTICLE
10.1029/2022JC019434

Multiple Abyssal Jets Flowing Into the Vema Deep, Romanche Fracture Zone

D. I. Frey[1,2,3], V. A. Krechik[1,4], L. D. Bashirova[1,4], S. A. Ostroumova[1], D. A. Smirnova[1,5], L. A. Kuleshova[1], E. P. Ponomarenko[1], E. G. Morozov[1,2,3], M. Ligi[6], I. Yu. Dudkov[1,4], and V. V. Sivkov[1,4]

[1]Shirshov Institute of Oceanology, Russian Academy of Sciences, Moscow, Russia, [2]Marine Hydrophysical Institute, Russian Academy of Sciences, Sevastopol, Russia, [3]Moscow Institute of Physics and Technology, Dolgoprudny, Russia, [4]Immanuel Kant Baltic Federal University, Kaliningrad, Russia, [5]Moscow State University, Moscow, Russia, [6]Italian National Research Council, Institute of Marine Science, Bologna, Italy

Key Points:

- Flow of the Antarctic Bottom Water (AABW) in the Romanche Fracture Zone intensifies at the entrance to the Vema Deep
- The flow splits into multiple jets observed in three distinct channels of the fracture zone
- AABW temperatures in the Vema Deep increased by 0.066°C over the last 30 years

Correspondence to:

D. I. Frey,
dima.frey@gmail.com

Citation:

Frey, D. I., Krechik, V. A., Bashirova, L. D., Ostroumova, S. A., Smirnova, D. A., Kuleshova, L. A., et al. (2023). Multiple abyssal jets flowing into the Vema Deep, Romanche Fracture Zone. *Journal of Geophysical Research: Oceans*, *128*, e2022JC019434. https://doi.org/10.1029/2022JC019434

Received 31 OCT 2022
Accepted 10 JAN 2023

Author Contributions:

Conceptualization: D. I. Frey, L. D. Bashirova
Data curation: V. A. Krechik, E. P. Ponomarenko, M. Ligi
Funding acquisition: D. I. Frey, E. G. Morozov
Investigation: S. A. Ostroumova, D. A. Smirnova
Methodology: I. Yu. Dudkov
Project Administration: V. V. Sivkov
Resources: L. D. Bashirova
Software: V. A. Krechik
Supervision: E. G. Morozov
Visualization: S. A. Ostroumova, D. A. Smirnova, L. A. Kuleshova
Writing – original draft: D. I. Frey
Writing – review & editing: L. D. Bashirova, L. A. Kuleshova, E. P. Ponomarenko, E. G. Morozov, M. Ligi, I. Yu. Dudkov, V. V. Sivkov

© 2023. American Geophysical Union. All Rights Reserved.

Abstract

Strong acceleration of abyssal flows in narrow deep-water channels and fracture zones is a key feature of bottom circulation in the Atlantic Ocean. In the Equatorial Atlantic, these bottom currents transport Antarctic Bottom Water (AABW) over the Mid-Atlantic Ridge from west to east. The main pathway for Antarctic waters in this region is the Romanche Fracture Zone. The deepest point of this fracture zone is the Vema Deep; its maximum depth based on the published data is 7,856 m. This deep basin is filled by waters of Antarctic origin overflowing a sill in a narrow channel. During the expedition on the R/V *Akademik Ioffe* (August 2022), we revealed a strong flow in the middle part of the Romanche Fracture Zone and collected new data on thermohaline and kinematic structures of this gravity current. Our survey is the first observational evidence of the intense flow into the Vema Deep. At the sill, the flow splits into branches flowing through three distinct channels of intricate configuration located in the southern transform valley of the fracture zone. The northern channel is proved to be the main pathway of the coldest and densest bottom waters to the Vema Deep. We also found that vertical structure of the flow is presented by two individual jets, namely the deep and bottom jets. The total transport of AABW through the Romanche Fracture Zone at this location was estimated at 1.40 Sv; the velocities exceeding 10 cm/s were found at depths greater than 5,000 m.

Plain Language Summary

Abyssal basins of the Atlantic Ocean are filled with cold and dense Antarctic waters. Propagation of these waters plays an important role in the heat transport of the ocean and influences the Earth's climate. The most intense bottom currents of Antarctic waters are formed in the narrow abyssal channels connecting deep ocean basins. In particular, fracture zones of the Mid-Atlantic Ridge connect deep basins of the western and eastern Atlantic. The equatorial Romanche Fracture Zone is the deepest fracture zone in the tropical Atlantic and provides transport of the coldest bottom waters from the Brazil to the Guinea and Sierra Leone basins. Direct measurements from ships remain the main source of information about the structure of currents in the abyssal fracture zones. In this work, we present new field observations at the entrance to the Vema Deep, which is the deepest point of the Romanche Fracture Zone. New measurements revealed several jets of the Antarctic Bottom Water flow guided by distinct channels in the bottom topography. It was also shown that the location of the abyssal pycnocline affects the vertical structure of the abyssal currents in this region. Comparison with historical measurements shows an increase in bottom temperatures exceeding 0.06°C.

1. Introduction

The deepest layers of abyssal basins, trenches, and fracture zones (FZ) in the Atlantic Ocean are filled with the Antarctic Bottom Water (AABW) (Baines & Condie, 1998; Foster & Carmack, 1976). This water mass originates over shallow areas in the Southern Ocean during austral winter period (Orsi et al., 1999). Its formation process includes strong cooling and water salinification caused by low winter temperatures and intense ice formation. In the Atlantic sector of the Southern Ocean, these dense waters are produced mainly in the Weddell Sea. The main northward flow of AABW in the Atlantic is concentrated in its western part (Hogg, 2001; Morozov et al., 2021). After reaching the northern periphery of the Brazil Basin, this flow divides into two branches (Tarakanov et al., 2018). One branch crosses the Mid-Atlantic Ridge through the equatorial and tropical FZ (Heezen et al., 1964; Mantyla & Reid, 1983; Mercier & Speer, 1998; Messias et al., 1999; Morozov et al., 2018),

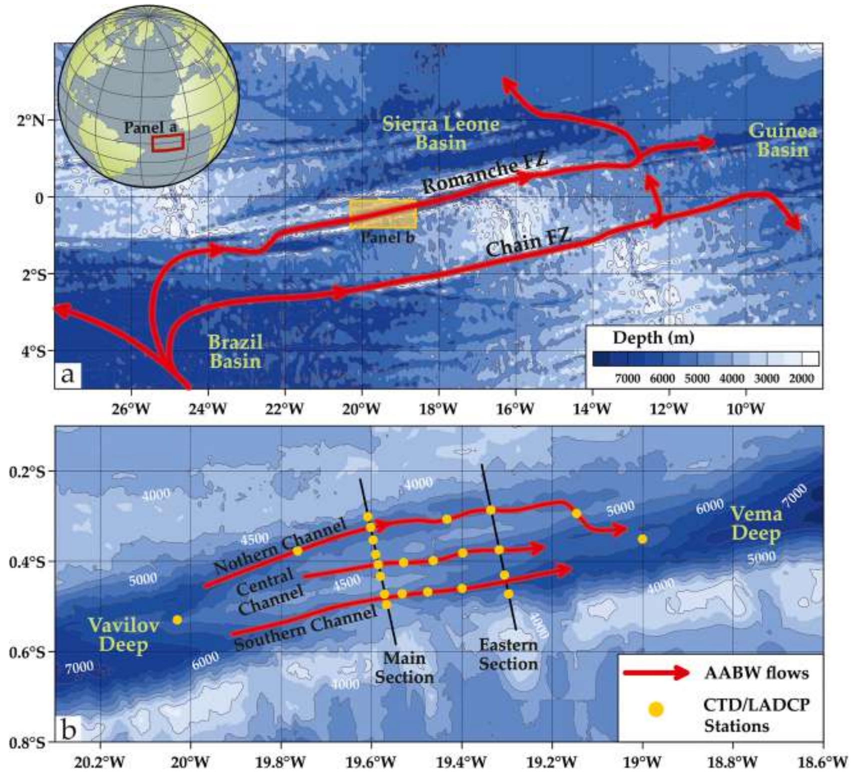

Figure 1. Mean bottom circulation schematic in the region of the Mid-Atlantic Ridge in the Equatorial Atlantic (panel a) and the region of our survey at the entrance to the Vema Deep (panel b). The main pathways of the Antarctic Bottom Water spreading are shown by red arrows. Our stations with Conductivity-Temperature-Depth and Lowered Acoustic Doppler Current Profiler measurements are indicated by yellow dots. The bottom topography is shown according to the General Bathymetric Chart of the Oceans 2022 database (a) and multibeam data (Bonatti et al., 1991; Efimov et al., 1996; Gasperini et al., 1997; Ligi et al., 2002) (b). The limits of the test site (b) are shown by red rectangle in panel (a).

and the other branch continues its northward propagation into the western Atlantic (Hall et al., 1997; Heezen et al., 1964; Limeburner et al., 2005; Mantyla & Reid, 1983; McCartney et al., 1991). The deepest FZ providing eastward transport of AABW in the tropical Atlantic are the Chain (1–2°S), Romanche (0–1°S), and Vema (11°N) FZ (Mantyla & Reid, 1983; Mercier & Speer, 1998; Morozov et al., 2018). In this work, we focus on the Romanche FZ which includes the deepest depression in the bottom topography of the Central Atlantic, namely, the Vema Deep (Figure 1).

The Romanche FZ is one of the longest (~950 km) transform of the mid-ocean ridge system located between 24°W and 13°W in the equatorial region (e.g., Bonatti et al., 1991). The transform represents a long-term stable feature and intrinsic element of the spreading process which transfers spreading from one segment of the ridge to the next (Gerya, 2010). The width of the Romanche FZ varies between 10 and 40 km. The fracture zone plays a leading role in a deep-water exchange between the Brazil and Guinea basins. A synthesis of available bathymetric data from the Romanche region revealed two narrow lens-shaped transform valleys: northern and southern (Ligi et al., 2002). The latter is namely a major valley with two depressions (western and eastern) with maximal depths of ~7,000 and ~7,800 m. The depressions are separated by a sill. Previously, the eastern one was named the Vema Deep after the R/V *Vema* (Heezen et al., 1964). The western one remains unnamed so far. Here, we suggest to name this depression "Vavilov Deep" in honor of the R/V *Akademik Sergey Vavilov*, onboard of which series of oceanographic measurements were carried out by the scientists of the Shirshov Institute of Oceanology in 2005–2016 (e.g., Tarakanov et al., 2013, 2018; Morozov et al., 2021).

The bottom topography is a baseline for designing the oceanographic survey. Thus, improving the accuracy and coverage of measured depths of the ocean floor is of a great importance. The bottom topography of the Romanche FZ has been repeatedly studied from the end of the 19th century, when the R/V *Romanche* made a 7,370 m sounding in the center of the Mid-Atlantic Ridge at 0.18°S, 18.25°W (0°11'S, 18°15'W) in 1883

(Heezen et al., 1964). Previously, Thomson (1878) postulated the existence of a central ridge dividing the Atlantic into two parallel troughs based on the few bottom temperature measurements performed during the H.M.S. *Challenger* (1872–1873) expedition. More detailed studies carried out during a *Meteor* expedition (1925–1926) indicated that the maximum sill depth across the Mid-Atlantic Ridge somewhat exceeds 4,000 m (Wüst, 1936). Subsequent measurements showed slightly different maximum depths in the Vema Deep region: 7,230 m from the vessel *Gauss* in 1901 (Drygalski, 1926), 7,600 m from the submarine *K-XVIII* in 1935 (Vening Meinesz, 1948), 7,728 m from the R/V *Albatross* in 1948 (Koczy, 1956), 7,856 from the R/V *Vema* in 1957 (Metcalf et al., 1964) and several other early estimates (see the review in Heezen et al. (1964)). In 1978 and 1983, GLORIA surveys of the Romanche transform and neighboring areas of the Equatorial Atlantic Ocean were carried out on the RRS *Discovery* and a new bathymetry chart was compiled (Searle et al., 1994). During the cruise of the R/V *Jean Charcot* in 1988, a ∼100-km long section of the Romanche FZ was surveyed at about 17°W and the SeaBeam bathymetric map was generated (Honnorez et al., 1991). The first detailed multibeam survey performed during the Romanche I expedition on the R/V *L'Atalante* in 1991 (Mercier et al., 1994; Monti & Mercier, 1991) covered a significant part of the Romanche FZ and allowed detailed studies of this fracture zone as a pathway for AABW spreading. A synthesis of previously mentioned bathymetric data was presented by Bonatti et al. (1991) and later compiled by Ligi et al. (2002) with multibeam coverage obtained during cruises of the R/V *Gelendzhik* in 1996 (Gasperini et al., 1997) and R/V *Akademik Nikolaj Strakhov* (1991–1992, 1993) (Efimov et al., 1996). As a result, a high-resolution digital terrain model (DTM) for the entire Romanche FZ has been developed. A detailed DTM for the western part of the Romanche FZ was generated based on data from the cruise of the R/V *Akademik Nikolaj Strakhov* (Kapustina et al., 2021). According to the DTM, the sill located at 1.1°S, 22.5°W (Tarakanov et al., 2013) serves as the AABW entrance from the Brazil Basin to the fracture zone and further east, into the Vavilov and Vema deeps. The maximum depth of the sill is 4,575 m (Kapustina et al., 2021). The Main Sill in the Romanche FZ is located at 13.68°W (13°41'W) with a minimum depth of 4,350 m (Mercier et al., 1994). It appears to be an exit of AABW flows from the fracture zone. According to Mercier and Morin (1997), the flow splits at 13.2°W (13°12'W) and circulates to the northeast filling the Sierra Leone Basin. Another part follows the Romanche transform valley toward the Guinea Basin (Figure 1).

Thermohaline structure of deep and bottom waters within the Romanche FZ is formed by two water masses: AABW below approximately 4,000 m depth and North Atlantic Deep Water (NADW) above this level (Mercier & Morin, 1997; Messias et al., 1999). These two water masses are divided by an abyssal pycnocline, which is more pronounced in the western part of the fracture zone. The upper limit of AABW in the equatorial zone is determined based on potential temperature isotherms of 1.8°C (Friedrichs & Hall, 1993; Macdonald, 1998), 1.9°C (McCartney & Curry, 1993; Whitehead & Worthington, 1982), and 2.0°C (Morozov et al., 2018; Wright, 1970). This limit is also determined in other publications by potential density isoline $\sigma_4 = 45.90$ kg/m^3 or neutral density isolines of 28.11 kg/m^3 (Ganachaud, 2003) or 28.141 kg/m^3 (Hernández-Guerra et al., 2014). In the Romanche FZ, isotherm 2°C of potential temperature approximately corresponds to salinity $S = 34.88$ psu, potential density $\sigma_4 = 45.86$ kg/m^3 or neutral density $\gamma^n = 28.106$ kg/m^3 (Morozov et al., 2021). Generally, the abyssal waters in the eastern Atlantic are more homogeneous and less dense than those of the western Atlantic; the difference in the bottom potential temperature between these basins can be as high as 1.5°C (Morozov et al., 2021). This change is caused by topographic blocking and intense mixing in the Romanche FZ (Ferron et al., 1998; Morozov et al., 2012; Tarakanov et al., 2018; van Haren et al., 2014). Note that both spatial and long-term temperature variations of AABW (Campos et al., 2021) should be taken into account while studying thermohaline properties of abyssal waters in the Atlantic. Conductivity-Temperature-Depth (CTD) measurements carried out in 1991 (Mercier & Morin, 1997), 2005 (Demidov et al., 2006), and 2009 (Morozov et al., 2010) allowed studies of the long-term potential temperature changes of bottom waters in the eastern part of the Romanche FZ. Thus, the minimum potential temperature at the bottom in 2009 (0.752°C) was higher by 0.057°C than in 1991 (0.695°C) and by 0.022°C higher than in 2005 (0.730°C) (Morozov et al., 2021). However, these measurements are located farther east of the Vema Deep. Meanwhile, at the entrance to the Vema Deep, there is an additional sill at 19.5°W, which was not studied earlier in terms of the intensification of AABW flow over the sill. Furthermore, by now, no CTD measurements were performed in the Vema Deep since French expeditions within the Romanche-I, Romanche-II, and Romanche-III projects in 1991–1994.

Kinematic structure of the AABW flows in the Romanche FZ was measured at several sills along the fracture zone; at such narrows, the bottom currents significantly accelerate (Whitehead, 1989, 1998). At the main sill at 13.68°W (13°41'W), four moorings were deployed for a period of two years from November 1992 to November

1994. Based on these measurements, the maximum time-averaged velocity and transports were estimated at 21 cm/s and 0.66 Sv, respectively (Mercier & Speer, 1998). Other estimates were up to 2 Sv (Polzin et al., 1996; Schlitzer, 1987; Warren & Speer, 1991). Direct Lowered Acoustic Doppler Current Profiler (LADCP) measurements carried out in 2005 and 2009 across the sills in the eastern part of the Romanche FZ revealed the AABW transports of 0.45 and 0.88 Sv, respectively (Demidov et al., 2006). At the western entrance to the fracture zone, the currents were measured using ADCPs both in profiling (Tarakanov et al., 2013) and moored (Tarakanov et al., 2018) modes. The maximum AABW velocities and transports were estimated at 48 cm/s and 0.35 Sv, respectively. Similar estimates of the AABW transports in the Romanche FZ were obtained using numerical model of abyssal flows (Frey et al., 2019); the model is described in detail in (Frey et al., 2017). Although numerous studies have been focused on the kinematic structure in the western and eastern parts of the Romanche FZ, there are no direct measurements along the flow between 22.5°W (the western entrance) and 16°W (one of the eastern sills), which is one of the main motivations of our expedition to the sill near the Vema Deep (19.5°W) carried out in August 2022.

The main goal of this paper is to study the horizontal and vertical structure of AABW in the Romanche FZ and intensity of its flow into the Vema Deep based on the new CTD and velocity data. A high-resolution DTM presenting a compilation of multibeam data collected during several scientific cruises served as the base for choosing the stations at the deepest points along the fracture zone. A detailed CTD and LADCP survey on transversal (across the Romanche transform system) and longitudinal (along the narrow parts of the southern transform valley) transects allowed quantifying the AABW transport into the Vema Deep and estimating the bottom temperature and salinity distributions at this part of the Romanche FZ.

2. Data and Methods

A detailed CTD/LADCP survey at the entrance to the Vema Deep was carried out during the 62nd cruise of the R/V *Akademik Ioffe* in August 2022. A high-resolution bottom topography generated from the multi-source bathymetric data (Bonatti et al., 1991; Efimov et al., 1996; Gasperini et al., 1997; Ligi et al., 2002) described in Section 2.1 was used as the basis for planning the oceanographic survey in the Romanche FZ. Section 2.2 is dedicated to our approach to CTD measurements and the equipment used in this survey; the LADCP data and data processing are presented in Section 2.3. The long-term variations of the thermohaline properties of AABW in the Vema Deep are analyzed in Section 2.4.

2.1. Bottom Topography Data

Bottom topography data of the Romanche FZ are available from the General Bathymetric Chart of the Oceans (GEBCO) data set which is a mixture of single-beam, multibeam, and satellite altimetry-derived bathymetry. From the first release of the GEBCO One Minute Grid in 2003, the quality of the data set has been significantly improved. Figure 2 illustrates the data set development through the GEBCO versions of the Romanche FZ bathymetry in 2014, 2021, and 2022 providing a global coverage with a grid resolution of 30 arcsec (~1 km) and 15 arcsec (~450 m), respectively. The main bathymetry source for the study site is presented by low-resolution indirect measurements (mostly predicted depths based on satellite-derived altimetry). Moreover, the percentage of the indirect measurements as a grid cell source is decreasing from 84.90% for the GEBCO 2014 grid to 68.07% and 66.99% for the GEBCO 2021 and GEBCO 2022 grids, respectively. However, the percentage of the cells based on more precise and detailed direct measurements has been steadily increasing from 15.10% for the GEBCO 2014 grid (5.36% multibeam echo sounding, 9.74% other methods) to 31.93% for the GEBCO 2021 grid (26.70% multibeam echo sounding, 5.23% other methods) and 33.01% for the GEBCO 2022 grid (28.31% multibeam echo sounding, 4.71% other methods). A comparison of the GEBCO bottom relief versions 2014 and 2022 shows that not a single passage, but two narrow channels are responsible for the deep-water exchange between the Vavilov and Vema deeps. A new detailed DTM of the entire Romanche FZ (Bonatti et al., 1991; Efimov et al., 1996; Gasperini et al., 1997; Ligi et al., 2002) with a spatial resolution of 10 arcsec (~200 m), allows distinguishing the third (southern) narrow channel (hereinafter, northern, central, and southern channels), as indicated by red lines in Figure 1b. The channels are located within the lens-shaped southern transform valley. They connect the Vavilov and Vema deeps appearing to be the passages for the eastward AABW flows.

An automatic classification and analysis of the DTM of the Romanche FZ were used to isolate the main thalweg (the line of the maximum depths) and the top lines of the walls (northern and southern) (Xiong et al., 2021). In this work, a digital terrain analysis was carried out using the GIS SAGA (Conrad et al., 2015) and GRASS GIS

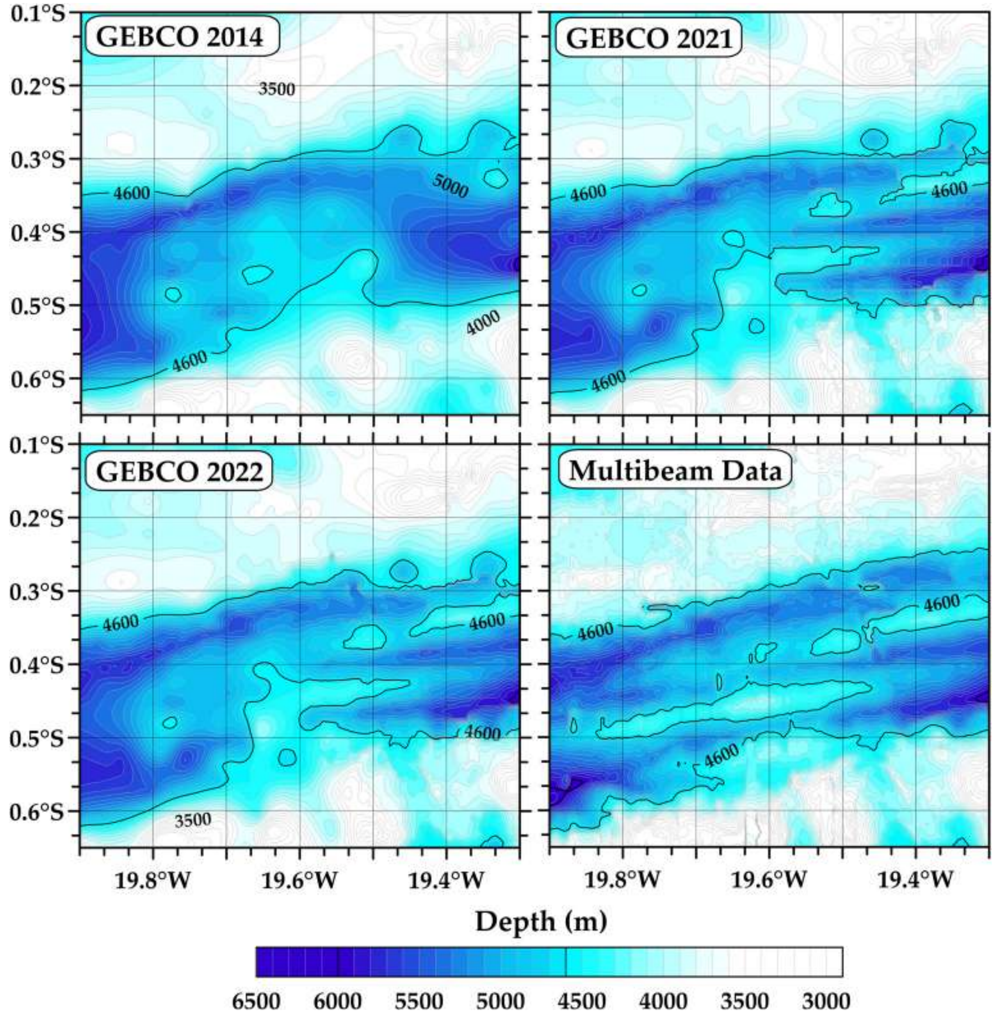

Figure 2. Comparison between the General Bathymetric Chart of the Oceans (GEBCO) databases (GEBCO, 2021, 2022) and the multibeam data (modified from Bonatti et al., 1991; Efimov et al., 1996; Gasperini et al., 1997; Ligi et al., 2002) covering the Romanche Fracture Zone region. The new multibeam data shows three distinct channels in the southern valley which are pathways of Antarctic Bottom Water inflow into the Vema Deep. One can see that the southern channel was not revealed by the GEBCO bathymetry data.

(Neteler & Mitasova, 2013) tools. At the first stage, the Basic Terrain Analysis module from the GIS SAGA was applied. The Channel Network parameter was chosen to distinguish the channel thalweg. The dominant waterflows were selected. The tops of the southern and northern walls of the fracture zone were defined using the Drainage Basins parameter, which limits the basins along the watersheds. At the second stage, a geomorphological classification of landforms was performed using the Geomorphons tool (Jasiewicz & Stepinski, 2013) from the GRASS GIS package. The results of the two previously mentioned approaches were compared to verify the close match of the Basic Terrain Analysis and the terrain morphology. Previously, the northern and southern walls, as well as the main thalweg, were allocated (Tarakanov et al., 2013) according to Smith and Sandwell (1997). Here, we present a detailed topographic profile along the southern and northern walls, and the main thalweg of the Romanche FZ based on the new multibeam data compilation. Different features (the maximum and minimum depths, width, basin area, length) of the main landforms were described to provide better understanding of the AABW pathways in the Romanche FZ (Figure 3).

2.2. CTD Measurements

In total, 23 full water depth stations (down to 5,865 m) were carried out in three channels of the sill between the Vavilov and Vema deeps; the entire data set is available at Frey et al. (2022). The rosette system General Oceanics

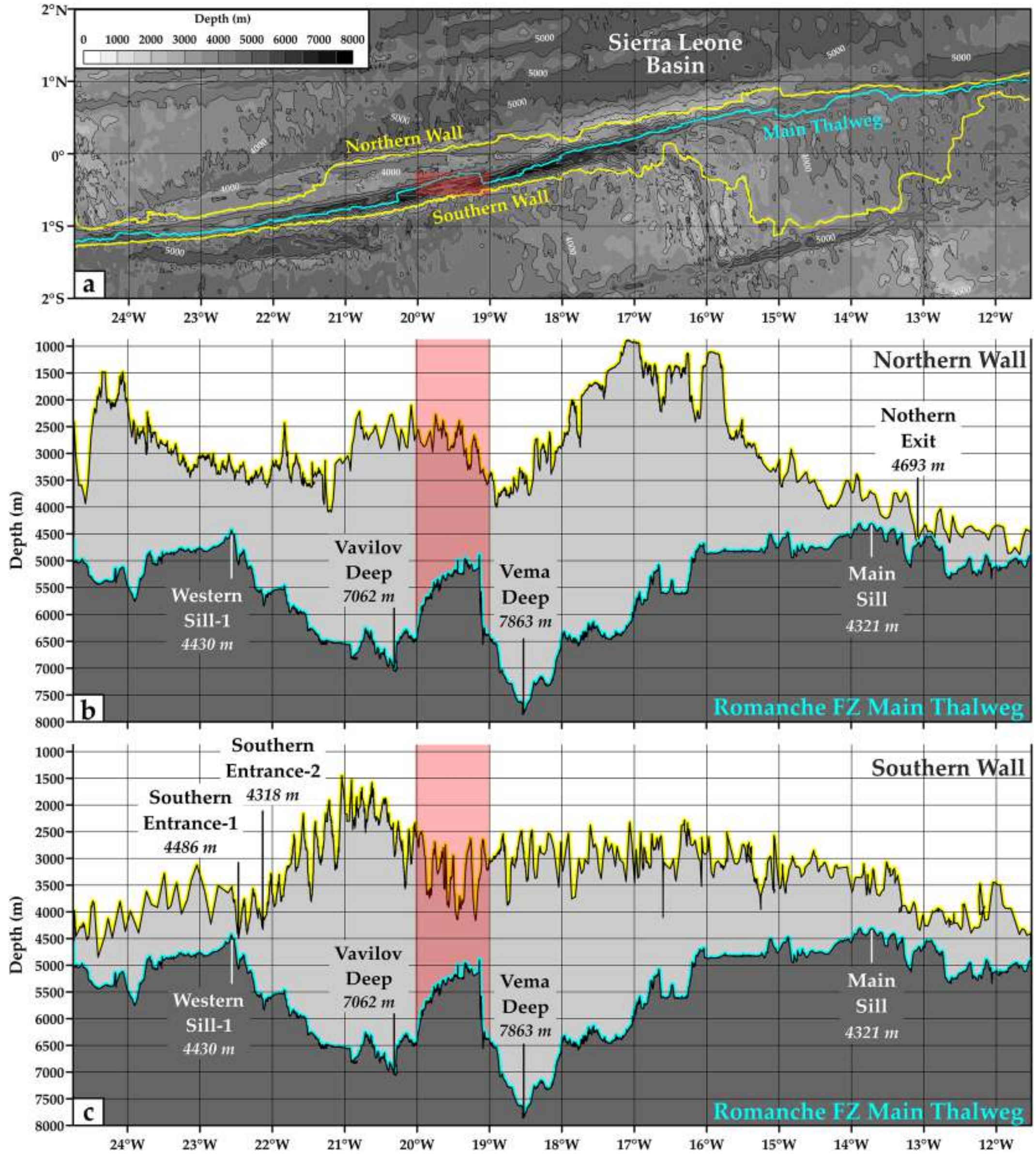

Figure 3. Bottom topography of the Romanche Fracture Zone based on the multibeam data (modified from Bonatti et al., 1991; Efimov et al., 1996; Gasperini et al., 1997; Ligi et al., 2002) (a), thalweg of the fracture together with depths of the northern (b) and southern (c) walls (modified from Tarakanov et al. (2013) based on the new bottom topography data). The region of the Conductivity-Temperature-Depth/Lowered Acoustic Doppler Current Profiler survey is shown by red rectangle in panel (a) and red band in panels (b,c).

GO1018 included Idronaut Ocean Seven 320 plus CTD probe and LADCP (300 kHz Teledyne RD Instruments WorkHorse Monitor with an external battery package), and 18 sampling Niskin bottles from 5 to 10-L capacity. We stopped the casts at a distance of 5 m above the bottom using the altimeter (model Valeport VA500) and pinger of the Benthos Co. Another pinger of our own construction was mounted on the rosette system for quick battery replacement. The combined use of pingers and an altimeter allowed us to safely approach the bottom even in conditions of rough bottom topography. A 6,000 m long sea cable allowed measurements at any point of the sill. It should be noted that it was not possible to measure currents in the bottom layer of the Vema Deep as its maximum depth exceeds 7,500 m; however, the intensification of AABW flows occurs at the narrow entrance to this depression and our study focuses on these relatively fast gravity currents. During profiling at the stations, the ship maintained its position with an accuracy of no less than 100 m.

Table 1
Locations of CTD Profiles at the Entrance to the Vema Deep of the Romanche Fracture Zone on 13–18 August 2022

Station number	Date/time (UTC)	Coordinates	CTD depth, m/ Ocean depth, m
AI62023	13.08.2022 15:05	20.029°W, 0.532°S	5,666/5,673
AI62024	13.08.2022 21:45	19.763°W, 0.378°S	5,439/5,444
AI62025	14.08.2022 03:04	19.607°W, 0.302°S	4,967/4,974
AI62026	14.08.2022 07:06	19.602°W, 0.325°S	5,373/5,383
AI62027	14.08.2022 11:05	19.596°W, 0.355°S	4,994/4,999
AI62028	14.08.2022 14:45	19.589°W, 0.384°S	4,714/4,721
AI62029	14.08.2022 18:37	19.585°W, 0.407°S	4,963/4,970
AI62030	14.08.2022 22:20	19.579°W, 0.434°S	4,430/4,438
AI62031	15.08.2022 02:01	19.572°W, 0.472°S	4,799/4,806
AI62032	15.08.2022 05:32	19.566°W, 0.496°S	4,351/4,358
AI62033	15.08.2022 09:01	19.532°W, 0.472°S	4,917/4,924
AI62034	15.08.2022 13:03	19.476°W, 0.468°S	5,351/5,358
AI62035	15.08.2022 17:26	19.399°W, 0.460°S	5,622/5,632
AI62036	15.08.2022 21:57	19.299°W, 0.472°S	4,880/4,887
AI62037	16.08.2022 02:22	19.308°W, 0.430°S	5,865/5,872
AI62038	16.08.2022 07:01	19.318°W, 0.375°S	5,541/5,551
AI62039	16.08.2022 11:10	19.337°W, 0.286°S	4,936/4,943
AI62040	16.08.2022 07:06	19.434°W, 0.308°S	5,073/5,080
AI62041	16.08.2022 20:27	19.529°W, 0.403°S	4,999/5,006
AI62042	17.08.2022 00:33	19.463°W, 0.399°S	5,266/5,272
AI62043	17.08.2022 08:21	19.398°W, 0.381°S	5,372/5,380
AI62044	17.08.2022 15:00	19.146°W, 0.294°S	4,911/4,918
AI62045	17.08.2022 20:20	19.000°W, 0.351°S	5,750/5,757

Note. All measurements were performed from the surface to the bottom; the exact depths are presented in the Table. Locations were selected based on the multibeam data (Bonatti et al., 1991; Efimov et al., 1996; Gasperini et al., 1997; Ligi et al., 2002). All CTD profiles were accompanied by LADCP measurements. The UTC time corresponds to the moment when the CTD and LADCP were near the bottom. Ocean depths are presented based on the CTD data combined with the altimeter records. CTD, Conductivity-Temperature-Depth; LADCP; Lowered Acoustic Doppler Current Profiler.

The exact locations, times and depths of stations are presented in Table 1. The locations were selected based on the multibeam topography data; in particular, the major part of the stations was located along the thalweg of each channel of the sill. The main section across the fracture zone included eight stations (62025–62032) at a distance of 2.5–4.3 km from each other. Two stations 62023 and 62045 were located to the west and east of the study site in the adjacent Vavilov and Vema deeps. Date and time are indicated for the moment when the CTD was near the bottom; the ocean depth was determined based on the CTD pressure and altimeter records. Each station took approximately 4 hr (the descent and ascent rates of the CTD and LADCP profilers were 1 m/s); the entire survey took 4.5 days.

The raw CTD data were collected and processed using standard Idronaut REDAS5 software version 5.78. The CTD data were transferred to conservative temperature (C_T) and absolute salinity (S_A) units using TEOS10 equations (Feistel, 2012) in Ocean Data View software version 5.2.0. We also used the data of several stations from the World Ocean Database 2018 (WOD-18) collected in the early 1990s in the Romanche FZ. The data from these stations were also recalculated using TEOS10 equations.

2.3. LADCP Measurements, Calibration, and Data Processing

The velocity profiles were measured by the LADCP RDI WorkHorse Monitor 300 kHz. The profiler was set in the narrowband mode, which increases the profiling range in comparison with the broadband mode and allows more reliable processing of the raw data. We set 30 vertical bins of 8 m each with 1.76 m blank distance immediately below the transducer. The LADCP compass was calibrated on land before the cruise in the down-looking mode according to the standard procedure. The raw data were processed using the LDEO Software version IX_14 (Visbeck, 2002). The magnetic declination was calculated in the frame of the processing package using the modern International Geomagnetic Reference Field (IGRF) model (Alken et al., 2021); the averaged declination in the survey area was estimated at −12.5°. The velocity error is also a result of processing the data using the specified software. In the bottom layer up to 150 m from the bottom, where the RDI BottomTrack operates, the error of the baroclinic velocity component is 1–2 cm/s. The results of processing were corrected by subtracting the tidal velocities using the TPXO9 model (Egbert & Erofeeva, 2002); the moment when the LADCP was near the bottom was used for these calculations. Usually, the velocities of the bottom currents exceed the tidal velocities by one order of magnitude; the typical tidal magnitudes of velocities are 1–2 cm/s. Note that the TPXO is a barotropic model and actual tidal velocities in a narrow abyssal channel can significantly differ from these estimated values. However, as the measured velocities are much higher than the tidal velocity, we can assume that the processed LADCP data reproduce mean currents in the fracture zone with sufficient accuracy.

3. Results

We analyzed abyssal bottom flows at the entrance to the Vema Deep based on the latest multi-source bathymetric data and new CTD and LADCP measurements performed in this region in August, 2022. The results are presented as follows. First, we provide information about the main features of the bottom topography and our approach to the selection of the positions of our CTD/LADCP casts (Section 3.1). Then, we analyze the transversal structure of the studied inflow (Section 3.2). In Section 3.3, we describe longitudinal variations of the inflow and evolution of the AABW properties along the studied region. Section 3.4 is dedicated to the long-term temperature and salinity variations of the bottom waters in the Vema Deep.

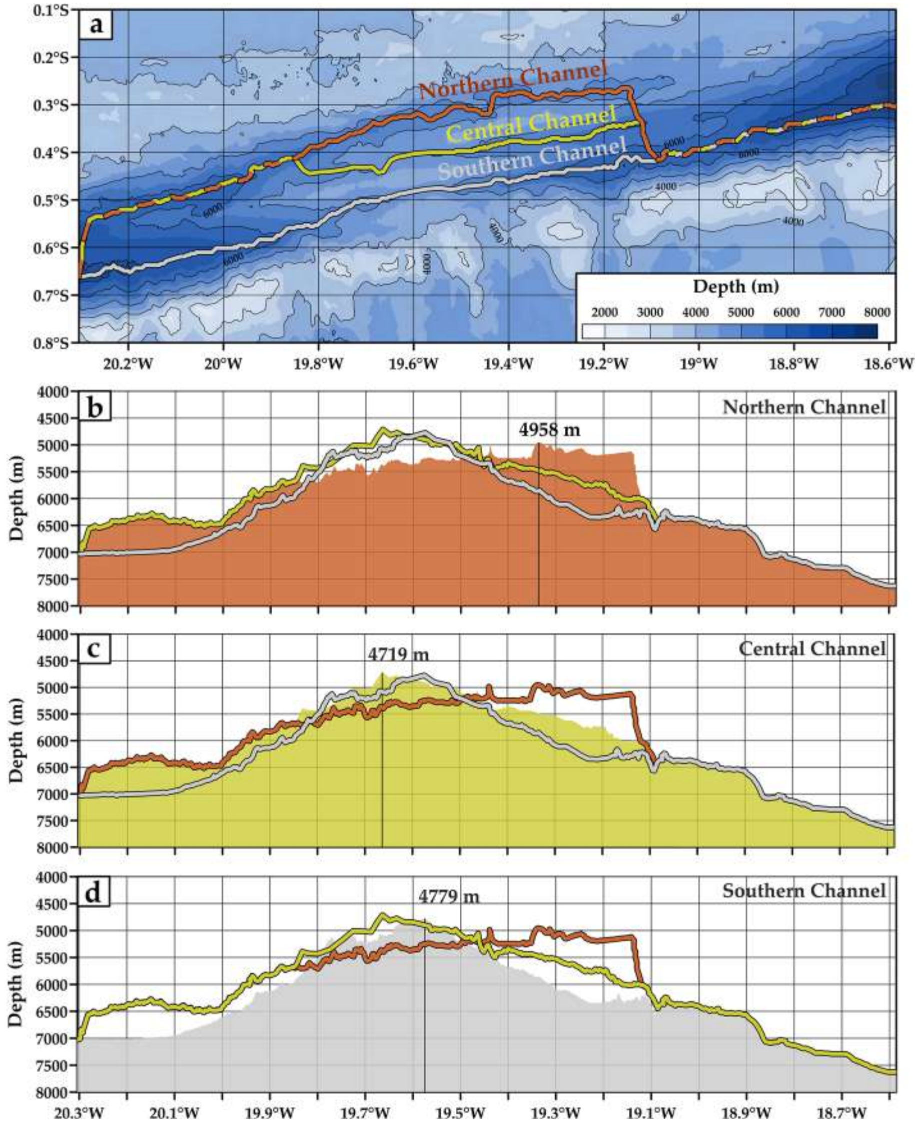

Figure 4. Comparison of the bottom topography profiles over the sill between the Vavilov and Vema deeps (a) and thalwegs of the northern (b), central (c), and southern (d) channels of this sill (each indicated by different colors). The northern channel is the deepest passage for the waters spreading into the Vema Deep.

3.1. Bottom Topography Data Analysis

The AABW pathways along the Romanche FZ were studied based on the precise data on bottom topography described in Section 2.1 in detail. Along the main thalweg, the following landforms were distinguished: the western sill, the Vavilov and Vema deeps, and the main sill with the revised maximum depths of 4,430, 7,062, 7,863, and 4,321 m, respectively. The Vavilov Deep is an elongated depression 345 km long and 27 km wide. An estimated total basin area covers ~5,900 km^2. The Vema Deep is 391 km long and 30 km wide with a total basin area of ~7,700 km^2. Between the Vavilov and Vema deeps there is a sill with three quasi-zonal channels deeper than 4,700 m (Figure 4). The northern channel is the deepest passage (4,958 m) for the waters spreading into the Vema Deep; its length is ~96 km. The central (~86 km long) and southern (~82 km long) channels do not exceed depths of 4,719 and 4,779 m at the sill, respectively.

3.2. Transversal Structure of the Flow Into the Vema Deep

The transversal structure of the flow along the Romanche FZ was studied based on two sections, namely the main and eastern sections, covering the entire fracture zone between its northern and southern walls (see Figure 1 for

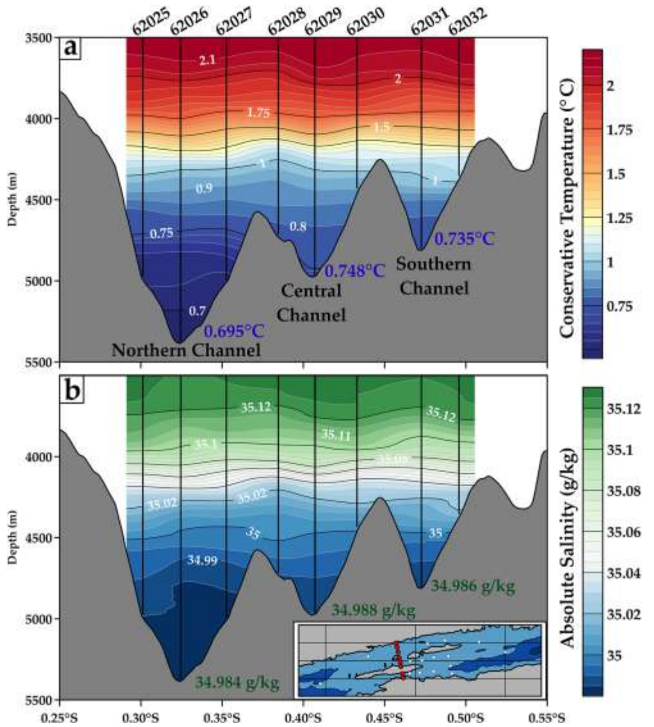

Figure 5. Conservative temperature (a) and absolute salinity (b) distributions at the main section across the Romanche Fracture Zone. The locations of the Conductivity-Temperature-Depth/Lowered Acoustic Doppler Current Profiler casts are shown in the inset of the bottom panel. Station numbers are indicated along the upper axis in panel (a). The ocean bottom is shown by gray color based on the multibeam data.

location of the sections). Both sections were oriented strictly perpendicular to the orientation of the transform valley; the exact deviation of the section lines from the meridional direction was 13° counterclockwise. The main section included eight stations at the narrowest place of the sill between the Vavilov and Vema deeps; the distance between stations varied between 2.5 and 4.3 km. This section crossed all three channels which provide AABW transports. Their maximum depths at the sill are 5,383 m (northern channel, station 62026), 4,970 m (central channel, station 62029), and 4,806 m (southern channel, station 62031). Note that the shallowest point of the northern channel is located 30 km downstream; its depth is 4,943 m (see Figure 4 for detailed thalwegs along each channel). Station 62,039 was located at this shallowest point; the eastern section crossed it strictly parallel to the main section. This eastern section consisted of four stations (62036–62039) and repeated the French section in August 1991, which allowed us to compare the long-term changes in thermohaline properties of bottom waters on the decadal time scale. Another station 62045 was carried out at a depth of 5,757 m in the Vema Deep at the section in 1994 allowing additional comparison with the historical CTD data set.

Conservative temperature and absolute salinity distributions showed similar patterns at the main section (Figure 5). The coldest (0.695°C), least saline (34.984 g/kg), and densest (46.056 kg/m^3) waters are transported through the northern channel. In the other two channels, the corresponding extremum values are 0.748°C, 34.988 g/kg, 46.050 kg/m^3 in the central channel, and 0.735°C, 34.986 g/kg, 46.050 kg/m^3 in the southern channel. Interestingly, the shallowest southern channel provides transport of colder (by 0.013°C) AABW than the central channel, which is 164 m deeper. Hence, more intense AABW currents exist in the southern channel, which will be discussed below based on the LADCP data. Above 4,500 m, the conservative temperature and absolute salinity isolines were relatively horizontal, which is typical for the abyssal currents near the Equator (Frey et al., 2019) as the Coriolis force and influence of bottom Ekman layer (Ekman, 1905) are insignificant. At higher latitudes, inclinations of isotherms in the bottom layer are essential in the case of intense abyssal flows (Jungclaus & Vanicek, 1999). An abyssal thermocline (pycnocline) between AADW and NADW was revealed at 3,700–4,200 m depths; no significant changes in its thickness and depth were observed from station to station. According to the published data, this pycnocline becomes less prominent in the eastern part of the Romanche FZ due to mixing over the eastern sills (Mercier & Morin, 1997). As for the region of our survey, the upper limit of the pycnocline is located at 3,700 m and corresponds to 1.9°C–2.0°C potential temperature isotherms, the lower limit is located at 4,200 m and corresponds to 1.1°C–1.2°C isotherms.

The kinematic structure of the flow was studied based on the LADCP profiles at the main section across the Romanche FZ (Figure 6). The velocities were projected to the direction along the fracture zone. The main peculiarity of the transversal kinematic structure is the presence of two individual branches of the AABW flow, namely the deep and bottom jets. The bottom jets are located in the deepest layer of the central and southern channels. The velocities of these jets increase toward the bottom and reach 7 cm/s in the central and 13 cm/s in the southern channel. As for the northern channel, a local maximum of 8 cm/s is located at a depth of 4,512 m, which corresponds to the shallowest sill of this channel located farther downstream. Thus, all three channels provide the AABW transports to the Vema Deep in the bottom layer.

Above the mentioned bottom jets, a layer of very low (less than 5 cm/s) or even opposite (up to 6 cm/s to the west) velocities are observed over the entire section. Above this low-velocity layer, the main deep jet of AABW is observed. This jet is located at depths between 3,700 and 4,300 m, which coincide very well with the 2°C conservative temperature isotherm and the depth of the main sill of the Romanche FZ, respectively. This main sill is located farther east at 13.68°W (13°41'W) and prevents free eastward spreading of deeper layers of Antarctic waters. This sill explains the existence of the no motion level deeper than 4,300 m. Deeper than this level, the

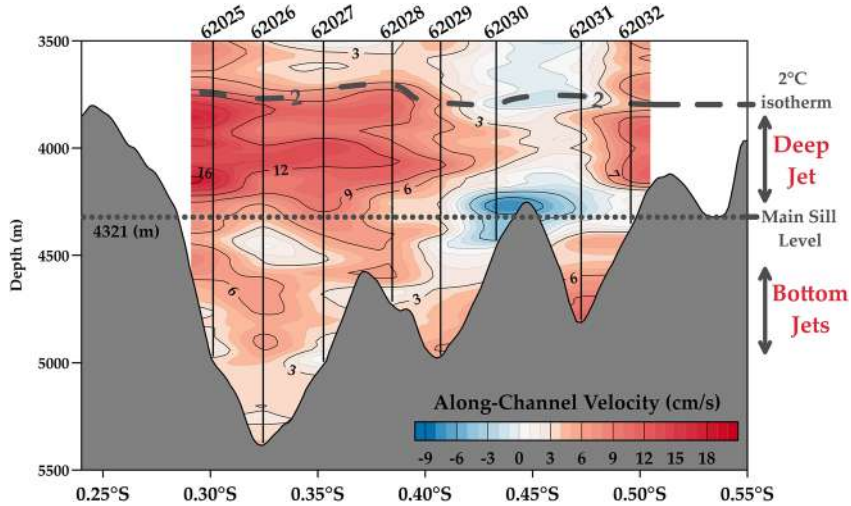

Figure 6. Distributions of along-channel velocity component at the main section across the Romanche Fracture Zone. Positive velocities correspond to the east-northeast direction (the exact value is 77° relative to the north). Locations of the Conductivity-Temperature-Depth/Lowered Acoustic Doppler Current Profiler casts are shown by thin solid lines; the station numbers are indicated along the upper axis. The ocean bottom is shown by gray color based on the multibeam data.

bottom jets correspond to local water exchange between the Vavilov and Vema deeps; the main sill located father to the east does not prevent this local intensification of currents between neighboring depressions.

Transports of deep and bottom jets at the main section were estimated based on the LADCP data. The transport of the deep jet between the 2°C potential temperature isotherm and the main sill level (4,321 m) is 0.98 Sv. The transports of the bottom jets calculated as the along-channels transports below the 4,321 m level are 0.28, 0.10, and 0.04 Sv through the northern, central, and southern channels, respectively. In total, 1.40 Sv of AABW with potential temperatures less than 2°C are transported into the Vema Deep.

CTD and LADCP data measured at the eastern section showed significantly different conservative temperature and velocity distributions (Figure 7) compared to the main section. First of all, the bottom topography significantly differs between two sections; the central and southern channels deepen to 5,551 and 6,090 m, respectively. On the contrary, the northern channel with a depth of 4,943 m is the shallowest sill at the eastern section; this sill is also the shallowest point along the entire northern channel between the Vavilov and Vema deeps. One can see that the AABW flow concentrates at the shallow northern channel; a sharp gradient in temperature is observed in the 200-m bottom layer, while the velocities in this layer are directed along the channel and reach 11 cm/s. The minimum conservative temperatures were 0.737°C and 0.736°C in the main and southern channels, respectively; in the northern channel, AABW was 0.039°C colder (Figure 7a). Velocities in bottom layers of the central and southern channels were low, less than 3 cm/s. However, significant eastward-directed jets exceeding 10 cm/s were observed above the seafloor at a depth of 4,700–5,000 m. These jets are formed at the sills over the main section and propagate to the east at a constant depth. At depths of 3,700–4,300 m, a continuation of the deep jet was observed. Similar to the main section, its maximum was displaced to the north and exceeded 10 cm/s. Note that the velocities of the deep jet in the eastern section were much lower than in the main sections. Two possible reasons of these low velocity are the displacement of the flow north of station 62039 or deceleration of the flow caused by widening of the fracture zone after the sill.

3.3. Longitudinal Structure of the Flow Into the Vema Deep

The longitudinal variations of the ABBW flow over the sill between the Vavilov and Vema deeps were studied based on three sections along each channel. Two background stations (62023 and 62045) were carried out in the deepest parts of the neighboring basins. In total, seven stations were performed along the thalweg of the northern channel; sections along the central and southern channels consist of five stations each. Bottom conservative temperature and velocities at all stations are presented in Figure 8. The total increase in bottom conservative temperature over the entire sill between the Vavilov and Vema deeps is 0.046°C or 0.40 mK/km (0.040°C per

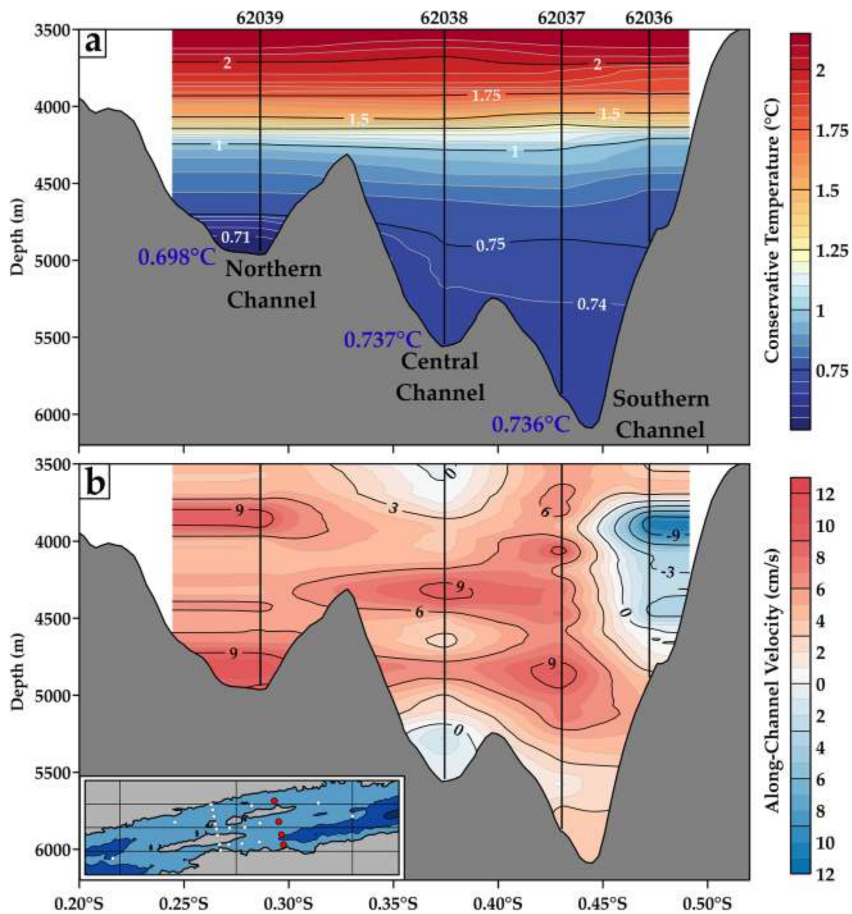

Figure 7. Conservative temperature (a) and along-channel (b) velocity distributions at the eastern section across the Romanche Fracture Zone. Locations of the Conductivity-Temperature-Depth/Lowered Acoustic Doppler Current Profiler casts are shown in the inset of the bottom panel. Station numbers are indicated along the upper axis in panel (a). The ocean bottom based on the multibeam data is shown by gray color.

100 km distance), indicating quite low rate of abyssal mixing. For comparison, the increase in bottom potential temperature between the entrance and exit of the Romanche FZ exceeds 1°C (more than 1.0 mK/km on average) (Morozov et al., 2021); the increase in the eastern part of the strait is 0.5°C/250 km (2.0 mK/km) (Ferron et al., 1998); the increase along the spillway in the western part of the fracture zone reaches 0.15°C (3.4 mK/km) (Tarakanov et al., 2018). However, even a value of 0.39 mK/km is quite high in comparison with other abyssal channels and especially abyssal basins; for instance, the horizontal gradient of potential temperature in the Vema Channel is less than 0.1 mK/km (Frey et al., 2018). It should be noted that the observed increase in bottom temperatures occurs east of 19.3°W after the main sill of the northern channel. Before the sill, the conservative temperature increases by no more than 0.005°C, while after the sill, the increase reaches 0.037°C.

Cross-channel changes in the bottom conservative temperature are much more significant than the changes in the longitudinal direction. Thus, the difference in minimum conservative temperatures between the northern and southern channels is 0.040°C at the main sill and 0.038°C at the eastern sill. As the Coriolis force is negligible, the observed differences are caused by the asymmetry of the bottom topography.

As for the velocity structure (Figure 8b), the eastward currents are clearly seen almost at all stations; the maximum speeds are 19 cm/s in the northern, 21 cm/s in the central, and 15 cm/s in the southern channel, indicating the importance of all channels to the bottom water exchange between the Vavilov and Vema deeps. Currents within the basins are slower; the velocities at the background stations 62023 and 62045 do not exceed 11 cm/s. Along the southern wall of the Romanche FZ, an opposite flow was observed at station 62036; the current speed reached 13 cm/s. However, as this westward flow is not observed in the narrowest part of the southern channel,

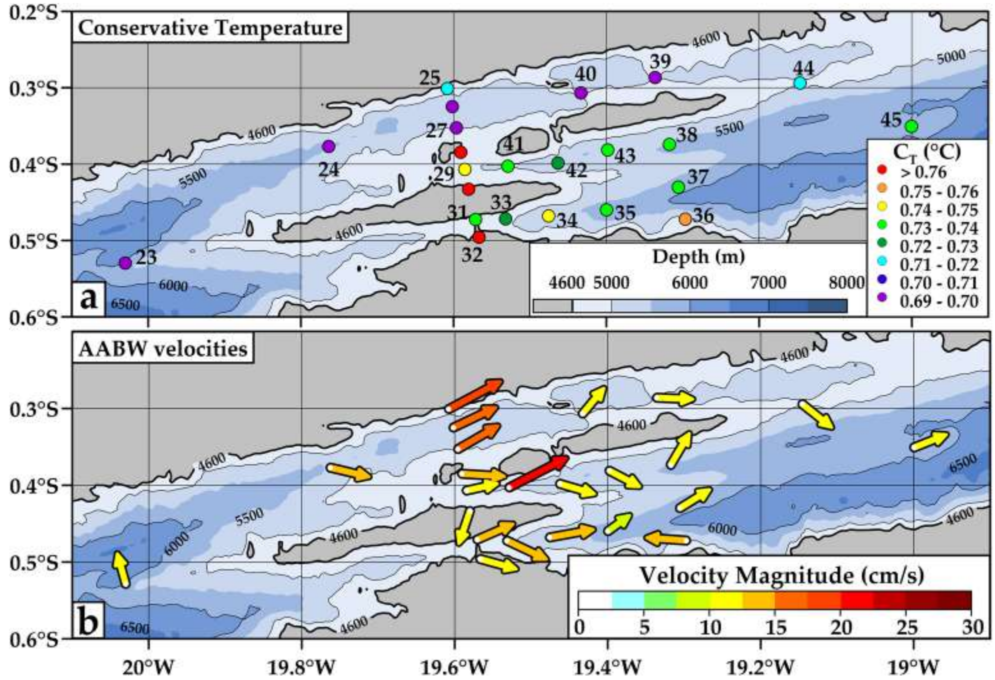

Figure 8. Bottom conservative temperature C_T (a) and maximum velocities in the Antarctic Bottom Water layer (b) in the study region based on our Conductivity-Temperature-Depth and Lowered Acoustic Doppler Current Profiler measurements. Conservative temperatures are presented from the deepest measurement at each station (5–7 m above the seafloor). The velocity was determined based on the maximum magnitude in the layer below the abyssal pycnocline and above the bottom. The area shallower than 4,600 m is shown by gray color based on the multibeam survey. The short variants of station numbers without the first three digits are indicated in panel (a).

we can conclude that this is a local current within the Vema Deep. Most likely, this flow does not contribute to the water exchange between neighboring deeps of the Romanche FZ.

Conservative temperature evolution along the northern (Figure 9), central and southern (Figure 10) channels were studied together with the longitudinal component of velocity. One can see that the conservative temperature does not change along the northern channel up to the shallowest sill at 19.337°W (station 62039). Exact values of the bottom conservative temperature are 0.689°C (station 62023), 0.693°C (station 62024), 0.695°C (station 62026), 0.700°C (station 62040), 0.698°C (station 62039). After the main sill, a fast bottom current is formed and intense mixing leads to a significant increase in conservative temperature, from 0.698°C (station 62039) to 0.718°C (station 62044) and 0.735°C (station 62045). Note that station 62045 is located in the wides part of the Vema Deep; thus, no significant changes in bottom temperature should be expected east of this station. This fact was confirmed by French measurements in the early 1990s, when several measurements were performed along the Romanche FZ (Mercier & Morin, 1997). As for the bottom velocities, they are quite low before the main sill (2 cm/s at station 62023, 5 cm/s at station 62024, and 5 cm/s at station 62026), become high nearly the shallowest sill (11 cm/s at station 62040, 12 cm/s at station 62039, 8 cm/s at station 62044), and finally, the bottom flow slows down and the velocity at station 62045 is 3 cm/s. The structure of the deep jet at 3,700–4,300 m is totally different. This current can be seen at all stations independently of the local sills of the northern channel; thus, its maximum velocity is 9 cm/s before the sill (station 62023), 15 cm/s in the middle part (station 62026), and 11 cm/s after the sill (station 62045). Some low velocities of the deep jet measured at some stations are probably caused by the meandering of the flow relative to the thalweg of the channel rather than actual slowdowns of the deep jet.

Sections along the thalwegs of the central and southern channels were made with much higher resolution (Figure 10); the distance between the neighboring stations varied between 4.1 and 10.7 km. In the central and southern channels, relatively slow spillway flows were found; a similar but much faster spillway was previously found at the entrance to the Romanche FZ (Tarakanov et al., 2018). In the central channel, the flow accelerates after overflowing the sill (the maximum velocity is 21 cm/s at station 62041) and then splits into three jets located

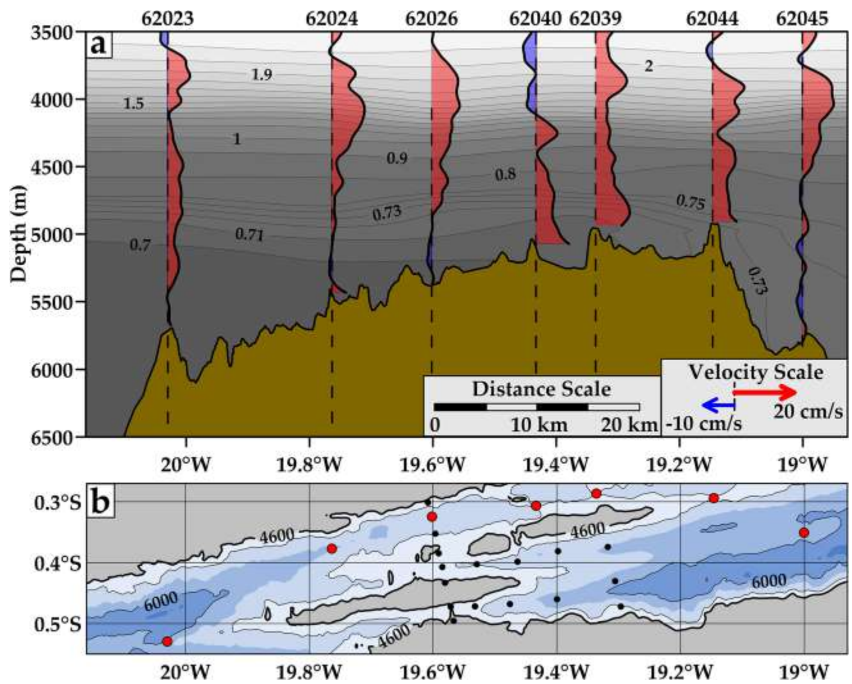

Figure 9. Conservative temperature distribution (shown in shades of gray) along the flow in the northern channel of the sill. Station numbers are indicated along the upper axis. Profiles of Lowered Acoustic Doppler Current Profiler along-channel velocity components are shown at each station by red (positive velocities are directed to the Vema Deep along the thalweg) and blue (negative velocities in the opposite direction) shading. The velocity scale is the same for all profiles and presented in the lower right corner. The ocean bottom is shown by deep yellow based on the multibeam data. Location of the stations over the section is shown in the bottom panel by red points.

at 4,510 (12 cm/s), 4,830 (6 cm/s) and 5,250 m (10 cm/s) observed at station 62042. Farther downstream, high velocities are observed in layer 4,500–5,000 m, but there are no significant currents below the 4,500 m level. The structure of currents along the southern channel is quite similar. The flow accelerates in the bottom layer up to 12 cm/s at station 62033 and then is observed at some distance above the bottom. Near the bottom, an opposite current with the maximum velocities up to 6 cm/s was found.

As for temperature changes, the minimum bottom conservative temperature changes from 0.740°C at station 62034 to 0.737°C at station 62035 and 0.736°C at station 62037, indicating that the deepest layer is occupied by the waters propagating from the east after passing the northern channel. Similar variations of thermohaline properties are observed in the central channel. The main conclusion here is that the central and southern channels provide eastward transport of relatively warm AABW, while the coldest AABW propagates both eastward and westward after passing through the northern channel; Figure 8a also clearly demonstrates this circulation pattern.

3.4. Long-Term Variations of Thermohaline Water Properties in the Vema Deep

The long-term temperature variations in the AABW layer are a subject of numerous works. However, direct repeated measurements are extremely rare in the Romanche FZ, which was the motivation for our measurements in the Vema Deep. The eastern section consisted of four stations (36–39) repeated the French section carried out on 15–16 August 1991 from the R/V *L'Atalante*, allowing studies of long-term variations in the properties of abyssal waters in the Vema Deep. Occasionally, our stations in 2022 were performed on the same dates, on 15–16 August. In total, four stations were carried out in 2022 instead of five stations in 1991 along the same line between the northern and southern walls of the Romanche FZ. Three stations (62036, 62038, 62039) were performed at the same points as the previous measurements; station 62037 was displaced 1.6 km north along the section to a shallower point due to technical reasons. All stations were used for the analysis of temperature distributions in 1991 and 2022 (Figure 11).

As was pointed out in Section 3.3, the coldest waters propagate through the northern channel. Waters in this channel are 0.04°C colder than in the continuation of the southern channel, which is more than 1,000 m deeper. This

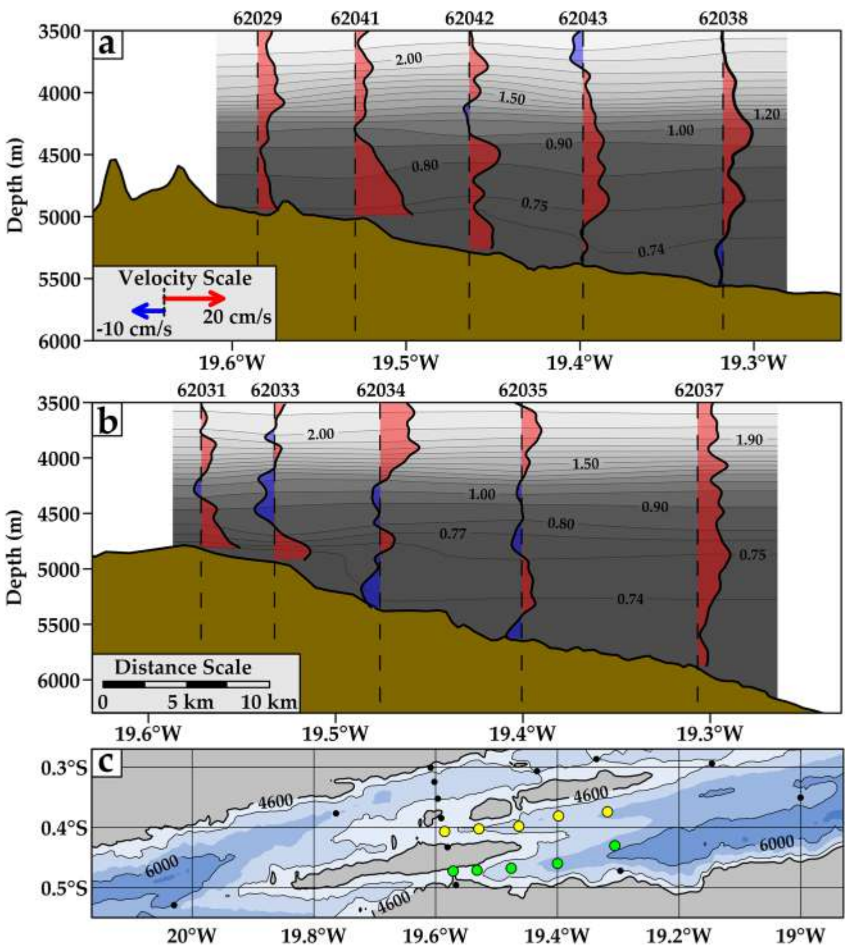

Figure 10. Conservative temperature distribution (shown in shades of gray) along the flow in the central (a) and southern (b) channels of the sill. Station numbers are indicated along the upper axes of (a) and (b) panels. Location of the stations over the section is shown in panel (c) by yellow (central section) and green (southern section) dots. Profiles of Lowered Acoustic Doppler Current Profiler along-channel velocity components are shown at each station by red (positive velocities are directed to the Vema Deep along the thalweg) and blue (negative velocities in the opposite direction) shading. The velocity scale is the same for all profiles and presented in the lower left corner of panel (a). The ocean bottom in panels (a) and (b) is shown by deep yellow color based on the multibeam data.

is a very uncommon temperature distribution caused by peculiarities of the bottom topography of the sill between the Vavilov and Vema deeps. This fact was confirmed by both surveys; a difference of 0.04°C is the same in 1991 and 2022. Conservative temperatures in the central and southern channels are the same; the 0.001°C difference is on the edge of the instrument accuracy. As can be seen from Figure 11c, the entire AABW layer below 4,000 m has become warmer; the average difference with the previous measurements is 0.06°C–0.07°C. Only a small area at the lower level of the abyssal pycnocline at a depth of 4,000 m became warmer by more than 0.1°C. It should be noted that temperatures near the bottom have increased by almost the same value in all three channels. Thus, the observed increase was 0.066°C in the central and northern channels and 0.065°C in the southern channel. This homogenous structure of bottom waters confirms the fact that the deepest layers of the central and southern channels are filled from the east by the waters from the northern channel. This circulation pattern leads to the observed identical warming of all bottom waters.

On the contrary, the NADW layer has generally become colder by the same value. Given that the relatively warm NADW layer has become colder, and the cold AADW layer has become warmer, we can assume that abyssal mixing between these two water masses intensified leading to the observed changes.

Another survey in the western part of the Vema Deep was carried out on 18 April 1994 from the R/V *Knorr*. In August 2022, we repeated one station from their section at a depth of 5,757 m. A comparison between two pairs

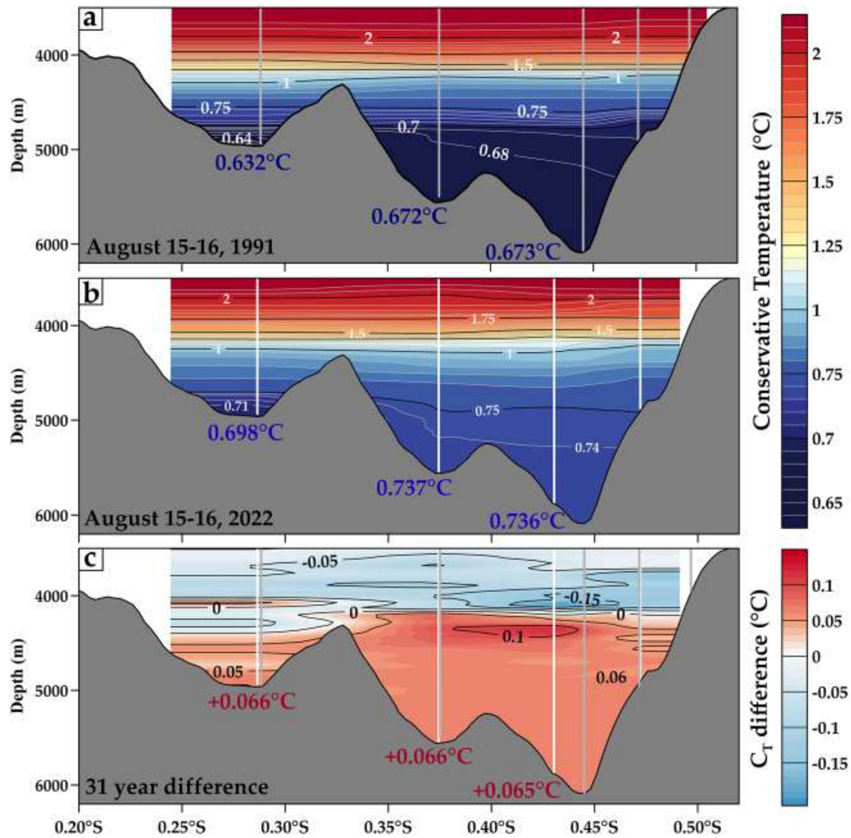

Figure 11. Conservative temperature (C_T) distributions measured in December 1991 (a) and August 2022 (b) at the section in the eastern part of the sill. Distribution of conservative temperature anomalies is shown in panel (c). The ocean bottom is shown based on the multibeam data. Exact values of the bottom conservative temperature are indicated by blue color at the bottom of each station; the 31-year differences between these values are indicated in panel (c) by red color. Locations of stations are shown by solid gray (stations in 1991) and white (stations in 2022) lines. The color scale for conservative temperature distributions is the same in (a) and (b) panels.

of stations is presented in Figure 12. Conservative temperature variations between profiles at 0.38°S, 19.32°W performed in 1991 and 2022 are shown in Figure 12a; the same comparison for stations at 0.35°S, 19.00°W performed in 1994 and 2022 is shown in Figure 12b. The results confirm previous conclusions about warming of the entire AABW layer from the abyssal pycnocline to the bottom. The bottom temperature at 19.32°W has become higher at 0.066°C; the increase at 19.00°W was 0.070°C. In contrast with stations at 19.32°W, no significant cooling of the NADW layers was observed at 19.00°W; instead, the depth of the pycnocline has decreased by approximately 155 m. Thus, it does not seem possible to determine the causes of the observed warming based on such scanty data; possible reasons are warming of the AABW waters, increased mixing, or changes in the intensity of bottom flows in the region.

4. Discussion

This study presents a new data set of direct measurements performed at one of the key points of the AABW spreading in the Romanche FZ. The survey covered the narrow sill between the Vavilov and Vema deeps. It is well known that acceleration of bottom flows occurs at such abyssal sills; the dynamics of these flows was studied theoretically (Whitehead, 1998; Whitehead et al., 1974) as well as by numerical simulations (Frey et al., 2019; Wadley & Bigg, 1995), laboratory experiments (Cossu et al., 2010; Davarpanah Jazi et al., 2020; Morozov et al., 2012), and field observations (see e.g., a review in Morozov et al. (2021)). Despite numerous works dedicated to the direct current observations of the AABW flows in the Romanche FZ, they were concentrated in the western (Tarakanov et al., 2013; van Haren et al., 2014) or eastern (Mercier & Speer, 1998) part of the fracture zone. The middle part of the fracture zone, including the sill west of the deepest depression of the Romanche

10.1029/2022JC019434

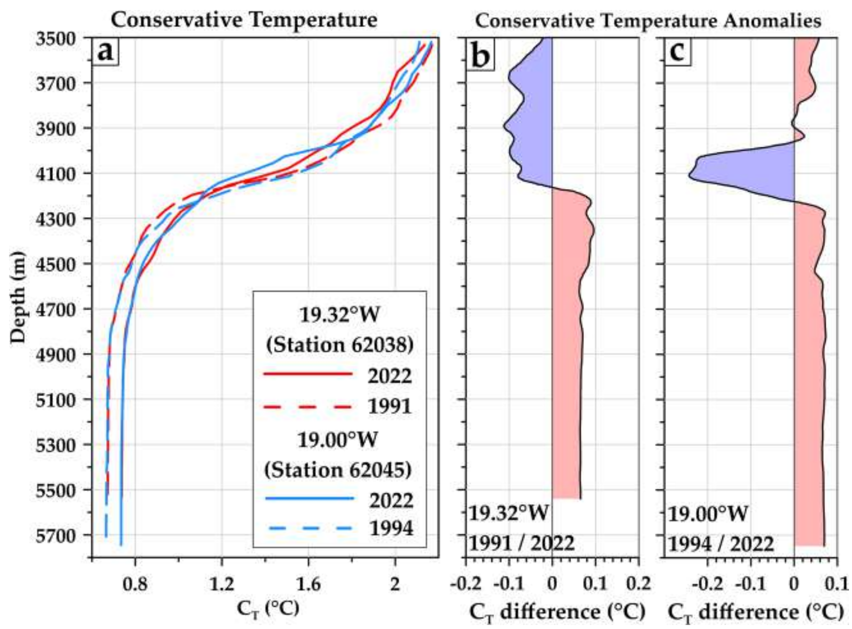

Figure 12. Comparison between conservative temperature (C_T) profiles measured in 1991 and 2022 at 0.38°S, 19.32°W and between profiles measured in 1994 and 2022 at 0.35°S, 19.00°W (a). Vertical distributions of conservative temperature anomalies are presented for both locations: at 19.32°W (b) and at 19.00°W (c).

FZ, was not covered by measurements, and our survey is the first observational evidence of intense currents in this region. These data allowed us to get new results of the AABW flow through the Romanche FZ, which are discussed below in the context of previous studies.

First of all, the analysis of a high-resolution DTM compilation based on a series of multibeam surveys revealed the intricate structure of the sill between two deepest basins of the Romanche FZ, namely the Vavilov and Vema deeps. Previously, a series of studies pointed out the importance of complex bathymetry in the Romanche FZ (Kapustina et al., 2021; Mercier and Speer, 1998; Tarakanov et al., 2018; van Haren et al., 2014). As for the studied sill at 19.5°W, no reliable information is available in the global bathymetry databases; even the modern GEBCO 2022 version (GEBCO, 2022) does not resolve all three passages for AABW jets over the sill. In addition, the detailed analysis of the new DTM compilation (Bonatti et al., 1991; Efimov et al., 1996; Gasperini et al., 1997; Ligi et al., 2002) allowed us to suppose that the northern channel is the pathway for the coldest and most intense AABW flow; later we confirmed this result by direct observations.

As was shown in Section 3.2, the abyssal flow into the Vema Deep splits into several distinct jets. Previous studies based on direct velocity measurements suggested a single core of the AABW flow in the Romanche FZ. In particular, a moored array deployed at 14.767°W (14°46’W) across the flow clearly shows the only velocity maximum at the center of the section between the walls of the fracture zone (Mercier & Speer, 1998). Similar structure is observed in the western part of the Romanche FZ based on LADCP measurements at five stations across the flow (Tarakanov et al., 2013). It should be noted that splitting of the AABW flow was observed in the spillway of the Romanche FZ (Morozov et al., 2012); however, this is a local effect and this peculiarity is not observed 30 km downstream based on the LADCP data mentioned above. Thus, the spatial structure of the current in the region between the Vavilov and Vema deeps significantly differs from previous measurements in the other parts of the fracture zone. Due to the greater depths and complex topography, the flow splits into three relatively slow bottom jets and one intense deep jet. This deep jet is limited by abyssal pycnocline from above and the main sill of the Romanche FZ from below (Figure 13). This main sill is located 650 km downstream.

As for the velocity magnitudes, a maximum value of 19.2 cm/s is observed in the deep jet at a depth of 4,150 m near the entrance to the Vema Deep at 19.5°W. This value agrees with the moored velocity measurements at 14.767°W (14°46’W), which yielded a maximum velocity of 21.7 cm/s in average, the depth of this maximum is 4,180 m (Mercier & Speer, 1998). Moreover, the LADCP measurements performed in the western part of the fracture zone at 22°10.5’ W show a maximum magnitude of 16.1 cm/s at 4,040 m depth (Tarakanov et al., 2013).

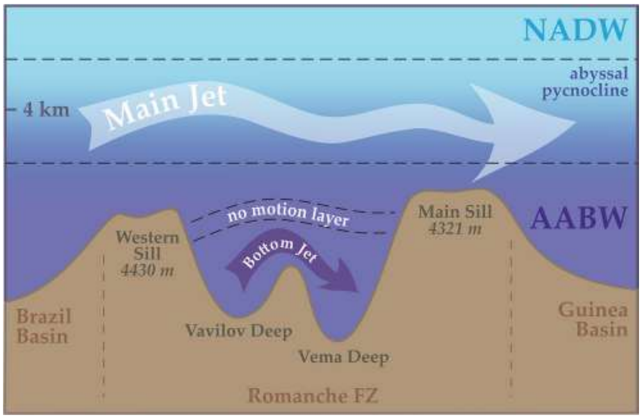

Figure 13. Schematic of the bottom and deep jets of the Antarctic Bottom Water flow over deep basins of the Romanche Fracture Zone.

Given that the velocities and depths of the deep jet are approximately the same in different parts of the Romanche FZ, we can suggest that this jet exists all over the pathway between the Brazil and Guinea basins, as indicated in Figure 13. The bottom jets at 19.5°W are local and provide transport only between the neighboring Vavilov and Vema deeps. It should be noted that much higher velocities were observed in the deep spillway at the entrance to the Romanche FZ at 22°30′W; the magnitudes reached 58 cm/s based on moored measurements and 48 cm/s by the LADCP data (Tarakanov et al., 2018). However, these values were obtained in a very narrow passage. After passing the spillway, the flow slows down to 16.1 cm/s, as was noted earlier.

Another important question is the observed warming of the bottom waters in the Vema Deep. As was shown in Section 3.4, the AABW layer has become warmer by 0.06°C–0.07°C between the early 1990s and 2022. By now, such measurements are extremely rare in this region and it is difficult to evaluate any trends in temperatures or causes of the observed warming. The only relevant data are the measurements carried out over the eastern sill of the Romanche FZ in 2005 and 2009 (Demidov et al., 2006; Morozov et al., 2010). These measurements repeated the French measurements performed in the early 1990s and resulted in almost the same values of the temperature increase (0.05°C–0.07°C). Almost the same potential temperature trend was observed in the Vema Channel at 31°S; the temperature increase during the last 30 years is approximately 0.06°C (Campos et al., 2021). However, the Antarctic waters propagate to the Equator during much longer time than 30 years and it is unlikely that this signal reached the Romanche FZ. While the age of the bottom waters in the northern Argentine Basin is approximately 30 years (Smythe-Wright & Boswell, 1998), the existing estimates for the age of bottom waters in the Northern Atlantic are approximately 275 (Stuiver et al., 1983) or 288 (Matsumoto, 2007) years. Thus, the temperature increase in the abyssal waters within the Romanche FZ is probably related to some local changes in the regime of abyssal circulation or increased mixing. Anyway, further measurements are important for studies of the variability of thermohaline and kinematic properties in the deepest layers of the Romanche FZ.

5. Summary and Conclusions

In this paper, we analyzed a set of recent CTD and LADCP measurements performed by the Shirshov Institute of Oceanology in the Romanche FZ in August, 2022. We focused on the overflow between the Vavilov and Vema deeps at 19–20°W. Based on these new data, we obtained the first observational evidence of the intense abyssal currents in this region and compared our results with the previous in situ measurements organized in different parts of the Romanche FZ. The results of this work are listed below:

1. The new DTM compiled from several multibeam surveys showed complex bathymetry of the sill between the Vavilov and Vema deeps not revealed by other topography databases. Three quasi-zonal channels deeper than 4,700 m were found at the sill; their topography and thalwegs were analyzed in the context of the AABW spreading along the Romanche FZ.
2. The detailed LADCP survey has shown the multi-jet structure of the AABW flow into the Vema Deep over the studied sill. Three bottom jets flow in each channel; one additional and most intense deep jet is observed at depths of the abyssal pycnocline. The comparison of our data with the historical ADCP and moored measurements suggest that this deep jet is observed along the entire Romanche FZ. This fact emphasizes the importance of the shallowest sill in the Romanche FZ at 13.68°W (13°41’W) as the main topographic barrier for the AABW flow between the Brazil and Guinea basins.
3. The measured maximum velocities of the bottom jets were 12 cm/s (northern channel), 21 cm/s (central channel), and 13 cm/s (southern channel); the maximum observed velocity of the deep jet was 19 cm/s. The comparison of our measurements with the historical data has shown that the velocity of the deep jet remains almost constant over the entire fracture zone. The AABW transports into the Vema Deep were estimated at 0.28 Sv (northern channel), 0.10 Sv (central channel), and 0.04 Sv (southern channel); the transport of the deep jet is 0.98 Sv. The total observed transport of AABW into the Vema Deep is 1.40 Sv.
4. The northern channel was proved to be the main source of bottom waters in the Vema Deep; it provides the transport of the coldest AABW flow. The spatial distribution of conservative temperature indicate that the

bottom water can spread westward (instead of general eastward direction) in a thin bottom layer after passing the northern channel. Local spillways were found in the central and southern channels similar to the previously observed deep spillway in the western part of the Romanche FZ.

5. The comparison with historical CTD data has shown an increase in the bottom temperatures of the entire AABW layer in the Vema Deep. An increase of 0.06°C–0.07°C over the last 30 years is almost constant for the layer deeper than the abyssal pycnocline. On the contrary, the deep layers of NADW have become colder, which may be an indication of changes in the flow regime and corresponding mixing in the deepest parts of the Romanche FZ.

Data Availability Statement

All experimental data used in the publication are available in open access through Mendeley (https://data.mendeley.com/datasets/xp3f7dzxnf/1); the entire data set and detailed description are available at Frey et al. (2022). Data processing and visualization were performed in Golden Software Surfer version 18.

Acknowledgments

We express our great appreciation to the crew of the R/V *Akademik Ioffe*, especially captain Andrey Zybin, who have supported our fieldworks. We are also grateful to Evgeny Krayushkin, the Technopole company and Idronaut support team for their help with our deep-water equipment. Ship operations, expenses, and data collection were funded by the state assignment of IO RAS (Theme FMWE-2021-0012); processing and interpretation of the in situ data were supported by the Russian Science Foundation (project 22-77-10004). M. Ligi was supported by the Italian National Program (PRIN_2017KY5ZX8). We thank the editor and two reviewers for providing comments that helped improving the final version of this paper.

References

Alken, P., Thébault, E., Beggan, C. D., Amit, H., Aubert, J., Baerenzung, J., et al. (2021). International geomagnetic reference field: The thirteenth generation. *Earth Planets and Space*, *73*(1), 49. https://doi.org/10.1186/s40623-020-01288-x

Baines, P. G., & Condie, S. (1998). Observation and modelling of Antarctic downslope flows: A review. In S. S. Jacobs & R. F. Weiss (Eds.), *Ocean, ice, and atmosphere: Interactions at the Antarctic continental margin* (Vol. 75, pp. 29–49). Antarctic Research Series. https://doi.org/10.1029/AR075p0029

Bonatti, E., Raznitsin, Y., Bortoluzzi, G., Boudillon, F., De Alteriis, G., Gasperini, L., et al. (1991). Geological studies of the eastern part of the Romanche transform (equatorial Atlantic): A first report. *Giornale di Geologia*, *53*(2), 31–48.

Campos, E. J., Van Caspel, M. C., Zenk, W., Morozov, E. G., Frey, D. I., Piola, A. R., et al. (2021). Warming trend in Antarctic Bottom Water in the Vema Channel in the South Atlantic. *Geophysical Research Letters*, *48*(19), e2021GL094709. https://doi.org/10.1029/2021GL094709

Conrad, O., Bechtel, B., Bock, M., Dietrich, H., Fischer, E., Gerlitz, L., et al. (2015). System for automated geoscientific analyses (SAGA), 2.1.4. *8*, 1991–2007. https://doi.org/10.5194/gmd-8-1991-2015

Cossu, R., Wells, M. G., & Wåhlin, A. K. (2010). Influence of the Coriolis force on the velocity structure of gravity currents in straight submarine channel systems. *Journal of Geophysical Research*, *115*(C11), C11016. https://doi.org/10.1029/2010JC006208

Davarpanah Jazi, S., Wells, M. G., Peakall, J., Dorrell, R. M., Thomas, R. E., Keevil, G. M., et al. (2020). Influence of Coriolis force upon bottom boundary layers in a large-scale gravity current experiment: Implications for evolution of sinuous deep-water channel systems. *Journal of Geophysical Research: Oceans*, *125*(3), e2019JC015284. https://doi.org/10.1029/2019JC015284

Demidov, A. N., Morozov, E. G., & Neiman, V. G. (2006). Structure and variability of deep waters in the Romanche fracture zone. *Doklady Earth Sciences*, *410*(1), 1136–1140. https://doi.org/10.1134/s1028334x06070300

Efimov, V. N., Sokolov, S. Y., Efimov, P. N., Gasperini, L., & Ligi, M. (1996). The structure of the transverse rise at the passive segment of the Romanche fracture zone. Doklady Akademii Nauk. *Earth Sciences Section*, *349*, 733–736.

Egbert, G. D., & Erofeeva, S. (2002). Efficient inverse modeling of barotropic ocean tides. *Journal of Atmospheric and Oceanic Technology*, *19*(2), 183–204. https://doi.org/10.1175/1520-0426(2002)019<0183:EIMOBO>2.0.CO;2

Ekman, V. W. (1905). On the influence of the earth's rotation on ocean-currents. *Arkiv för matematik, astronomi och fysik*, *2*, 1–53.

Feistel, R. (2012). TEOS-10: A new international oceanographic standard for seawater, ice, fluid water, and humid air. *International Journal of Thermophysics*, *33*(8–9), 1335–1351. https://doi.org/10.1007/s10765-010-0901-y

Ferron, B., Mercier, H., Speer, K., Gargett, A., & Polzin, K. (1998). Mixing in the Romanche fracture zone. *Journal of Physical Oceanography*, *28*(10), 1929–1945. https://doi.org/10.1175/1520-0485(1998)028<1929:MITRFZ>2.0.CO;2

Foster, T. D., & Carmack, E. C. (1976). Frontal zone mixing and Antarctic Bottom Water formation in the southern Weddell Sea. *Deep Sea Research*, *23*(4), 301–317. https://doi.org/10.1016/0011-7471(76)90872-X

Frey, D. I., Fomin, V. V., Diansky, N. A., Morozov, E. G., & Neiman, V. G. (2017). New model and field data on estimates of Antarctic Bottom Water flow through the deep Vema Channel. *Doklady Earth Sciences*, *474*(1), 561–564. https://doi.org/10.1134/S1028334X17050026

Frey, D. I., Fomin, V. V., Tarakanov, R. Y., Diansky, N. A., & Makarenko, N. I. (2018). Bottom water flows in the Vema channel and over the Santos plateau based on the field and numerical experiments. In M. G. Velarde, R. Y. Tarakanov, & A. V. Marchenko (Eds.), *The ocean in motion: Circulation, waves, polar oceanography* (pp. 475–485). Springer International Publishing. https://doi.org/10.1007/978-3-319-71934-4_29

Frey, D. I., Krechik, V. A., Bashirova, L. D., Ostroumova, S. A., Smirnova, D. A., & Morozov, E. G. (2022). CTD and LADCP measurements in the Romanche fracture zone during cruise 62 of the R/V Akademik Ioffe in August, 2022 [Dataset]. Mendeley Data. http://doi.org/10.17632/xp3f7dzxnf.1

Frey, D. I., Morozov, E. G., Fomin, V. V., Diansky, N. A., & Tarakanov, R. Y. (2019). Regional modeling of Antarctic Bottom Water flows in the key passages of the Atlantic. *Journal of Geophysical Research: Oceans*, *124*(11), 8414–8428. https://doi.org/10.1029/2019JC015315

Friedrichs, M. A., & Hall, M. M. (1993). Deep circulation in the tropical North Atlantic. *Journal of Marine Research*, *51*(4), 697–736. https://doi.org/10.1357/0022240933223909

Ganachaud, A. (2003). Large-scale mass transports, water mass formation, and diffusivities estimated from World Ocean circulation experiment (WOCE) hydrographic data. *Journal of Geophysical Research*, *108*(C7), 3213. https://doi.org/10.1029/2002JC001565

Gasperini, L., Bonatti, E., Ligi, M., Sartori, R., Borsetti, A. M., Negri, A., et al. (1997). Stratigraphic numerical modelling of a carbonate platform on the Romanche transverse ridge, Equatorial Atlantic. *Marine Geology*, *136*(3–4), 245–257. https://doi.org/10.1016/S0025-3227(96)00068-0

GEBCO Compilation Group. (2021). GEBCO 2021 grid. https://doi.org/10.5285/c6612cbe-50b3-0cff-e053-6c86abc09f8f

GEBCO Compilation Group. (2022). GEBCO_2022 grid. https://doi.org/10.5285/e0f0bb80-ab44-2739-e053-6c86abc0289c

Gerya, T. (2010). Dynamical instability produces transform faults at mid-ocean ridges. *Science*, *329*(5995), 1047–1050. https://doi.org/10.1126/science.1191349

Hall, M. M., McCartney, M., & Whitehead, J. A. (1997). Antarctic Bottom Water flux in the equatorial western Atlantic. *Journal of Physical Oceanography*, *27*(9), 1903–1926. https://doi.org/10.1175/1520-0485(1997)027<1903:ABWFIT>2.0.CO;2

Heezen, B. C., Bunce, E., Hersey, J., & Tharp, M. (1964). Chain and Romanche fracture zones. *Deep Sea Research*, *11*(1), 11–33. https://doi.org/10.1016/0011-7471(64)91079-4

Hernández-Guerra, A., Pelegrí, J. L., Fraile-Nuez, E., Benítez-Barrios, V., Emelianov, M., Pérez-Hernández, M. D., & Vélez-Belchí, P. (2014). Meridional overturning transports at 7.5 N and 24.5 N in the Atlantic Ocean during 1992–93 and 2010–11. *Progress in Oceanography*, *128*, 98–114. https://doi.org/10.1016/j.pocean.2014.08.016

Hogg, N. G. (2001). Quantification of the deep circulation. In G. Siedler, J. Church, & J. Gould (Eds.), *Ocean circulation and climate: Observing and modelling the global ocean* (Vol. 77, pp. 259–270). International Geophysics Series.

Honnorez, J., Mascle, J., Tricart, P., Villeneuve, M., & Bertrand, H. (1991). Mapping of a segment of the Romanche fracture zone: A morphostructural analysis of a major transform fault of the equatorial Atlantic Ocean. *Geology*, *19*(8), 795–798. https://doi.org/10.1130/0091-7613(1991)019<0795:MOASOT>2.3.CO;2

Jasiewicz, J., & Stepinski, T. (2013). Geomorphons—A pattern recognition approach to classification and mapping of landforms. *Geomorphology*, *182*, 147–156. https://doi.org/10.1016/j.geomorph.2012.11.005

Jungclaus, J., & Vanicek, M. (1999). Frictionally modified flow in a deep ocean channel: Application to the Vema Channel. *Journal of Geophysical Research*, *104*(C9), 21123–21136. https://doi.org/10.1029/1998jc900055

Kapustina, M. V., Dorokhov, D. V., & Sivkov, V. V. (2021). Multibeam bathymetry data of the western part of the Romanche trench (Equatorial Atlantic). *Data in Brief*, *37*, 107198. https://doi.org/10.1016/j.dib.2021.107198

Koczy, F. F. (1956). Echo soundings. In *Rep. Swedish Deep-Sea Exped., 1947–1948, 4. Bottom Investigations* (Vol. 2, pp. 99–158).

Ligi, M., Bonatti, E., Gasperini, L., & Poliakov, A. N. B. (2002). Oceanic broad multifault transform plate boundaries. *Geology*, *30*(1), 11–14. https://doi.org/10.1130/0091-7613(2002)030<0011:OBMTPB>2.0.CO;2

Limeburner, R., Whitehead, J. A., & Cenedese, C. (2005). Variability of Antarctic Bottom Water flow into the North Atlantic. *Deep Sea Research, Part II*, *52*(3–4), 495–512. https://doi.org/10.1016/j.dsr2.2004.12.012

Macdonald, A. (1998). The global ocean circulation a hydrographic estimate and regional analysis. *Progress in Oceanography*, *41*(3), 281–382. https://doi.org/10.1016/S0079-6611(98)00020-2

Mantyla, A. W., & Reid, J. L. (1983). Abyssal characteristics of the World Ocean waters. *Deep-Sea Research*, *30*(8), 805–833. https://doi.org/10.1016/0198-0149(83)90002-X

Matsumoto, K. (2007). Radiocarbon-based circulation age of the world oceans. *Journal of Geophysical Researc*h, *112*(C9), C09004. https://doi.org/10.1029/2007JC004095

McCartney, M. S., Bennet, S. L., & Woodgate-Jones, M. E. (1991). Eastward flow through the Mid-Atlantic Ridge at 11°N and its influence on the abyss of the eastern basin. *Journal of Physical Oceanography*, *21*(8), 1089–1121. https://doi.org/10.1175/1520-0485(1991)021<1089:EFTTMA>2.0.CO;2

McCartney, M. S., & Curry, R. A. (1993). Trans-equatorial flow of Antarctic Bottom Water in the western Atlantic Ocean: Abyssal geostrophy at the equator. *Journal of Physical Oceanography*, *23*(6), 1264–1276. https://doi.org/10.1175/1520-0485(1993)023<1264:TFOABW>2.0.CO;2

Mercier, H., & Morin, P. (1997). Hydrography of the Romanche and chain fracture zones. *Journal of Geophysical Research*, *102*(C5), 10373–10389. https://doi.org/10.1029/97JC00229

Mercier, H., & Speer, K. G. (1998). Transport of bottom water in the Romanche fracture zone and the chain fracture zone. *Journal of Physical Oceanography*, *28*(5), 779–790. https://doi.org/10.1175/1520-0485(1998)028<0779:TOBWIT>2.0.CO;2

Mercier, H., Speer, K. S., & Honnorez, J. (1994). Romanche flow pathways of bottom water through the Romanche and chain fracture zones. *Deep-Sea Research*, *41*(10), 1457–1477. https://doi.org/10.1016/0967-0637(94)90055-8

Messias, M.-J., Andrié, C., Mémery, L., & Mercier, H. (1999). Tracing the North Atlantic deep water through the Romanche and Chain fracture zones with chlorofluoromethanes. *Deep Sea Research Part I*, *46*(7), 1247–1278. https://doi.org/10.1016/S0967-0637(99)00005-9

Metcalf, W. G., Heezen, B. C., & Stalcup, M. C. (1964). The sill depth of the mid-Atlantic ridge in the equatorial region. *Deep Sea Research Part I*, *11*, 1–10. https://doi.org/10.1016/0011-7471(64)91078-2

Monti, S., & Mercier, H. (1991). Carte bathymetrique de la zone de fracture de la Romanche (Seabeam Em12). Cartographie, 1 sheet, scale 1:1 000 000.

Morozov, E. G., Demidov, A. N., Tarakanov, R. Y., & Zenk, W. (2010). Mode water. In G. Weatherly (Ed.), *Abyssal channels in the Atlantic Ocean: Water structure and flows* (p. 266). Springer.

Morozov, E. G., Tarakanov, R. Y., & Frey, D. I. (2021). *Bottom gravity currents and overflows in deep channels of the Atlantic Ocean observations, analysis, and modeling*. Springer Nature.

Morozov, E. G., Tarakanov, R. Y., Frey, D. I., Demidova, T. A., & Makarenko, N. I. (2018). Bottom water flows in the tropical fractures of the northern Mid-Atlantic Ridge. *Journal of Oceanography*, *74*(2), 147–167. https://doi.org/10.1007/s10872-017-0445-x

Morozov, E. G., Tarakanov, R. Y., Lyapidevskii, V. Y., & Makarenko, N. I. (2012). Abyssal cataracts in the Romanche and Chain fracture zones. *Doklady Earth Sciences*, *53*(6), 655–667. https://doi.org/10.1134/S1028334X12100091

Neteler, M., & Mitasova, H. (2013). *Open source GIS: A GRASS GIS approach* (Vol. 689, p. 420). Springer Science & Business Media.

Orsi, A. H., Johnsson, G. C., & Bullister, J. L. (1999). Circulation, mixing, and production of Antarctic Bottom Water. *Progress in Oceanography*, *43*(1), 55–109. https://doi.org/10.1016/s0079-6611(99)00004-x

Polzin, K. L., Speer, K. G., Toole, J. M., & Schmitt, R. W. (1996). Intense mixing of Antarctic Bottom Water in the equatorial Atlantic Ocean. *Nature*, *380*(6569), 54–57. https://doi.org/10.1038/380054a0

Schlitzer, R. (1987). Renewal rates of East Atlantic deep water estimated by inversion of 14C data. *Journal of Geophysical Research*, *92*(C3), 2953–2980. https://doi.org/10.1029/JC092iC03p02953

Searle, R. C., Thomas, M. V., & Jones, E. J. W. (1994). Morphology and tectonics of the Romanche transform and its environs. *Marine Geophysical Researches*, *16*(6), 427–453. https://doi.org/10.1007/bf01270518

Smith, W. H. F., & Sandwell, D. T. (1997). Global seafloor topography from satellite altimetry and ship depth soundings. *Science*, *277*(5334), 1956–1962. https://doi.org/10.1126/science.277.5334.1956

Smythe-Wright, D., & Boswell, S. (1998). Abyssal circulation in the Argentine basin. *Journal of Geophysical Research*, *103*(C8), 15845–15851. https://doi.org/10.1029/98JC00142

Stuiver, M., Quay, P. D., & Ostlund, H. G. (1983). Abyssal water carbon-14 distribution and the age of the world oceans. *Science*, *219*(4586), 849–851. https://doi.org/10.1126/science.219.4586.849

Tarakanov, R. Y., Makarenko, N. I., & Morozov, E. G. (2013). Antarctic bottom water flow in the western part of the Romanche fracture zone based on the measurements in October of 2011. *Oceanology*, *53*(6), 655–667. https://doi.org/10.1134/S0001437013050147

Tarakanov, R. Y., Morozov, E. G., van Haren, H., Makarenko, N. I., & Demidova, T. A. (2018). Structure of the deep spillway in the western part of the Romanche fracture zone. *Journal of Geophysical Research: Oceans*, *123*(11), 8505–8531. https://doi.org/10.1029/2018JC013961

Thomson, C. W. (1878). *The Voyage of the challenger, the Atlantic* (Vol. 2, pp. 246–326). Harper & Brothers.

van Haren, H., Gostiaux, L., Morozov, E., & Tarakanov, R. (2014). Extremely long Kelvin–Helmholtz billow trains in the Romanche fracture zone. *Geophysical Research Letters*, *41*(23), 8445–8451. https://doi.org/10.1002/2014GL062421

Vening Meinesz, F. A. (1948). *Gravity expeditions at sea, 1923–1938* (Vol. 4, p. 233). Netherlands Geodetic Commission Publishing.

Visbeck, M. (2002). Deep velocity profiling using lowered acoustic Doppler current profiler: Bottomtrack and inverse solution. *Journal of Atmospheric and Oceanic Technology*, *19*(5), 794–807. https://doi.org/10.1175/1520-0426(2002)019<0794:DVPULA>2.0.CO;2

von Drygalski, E. (1926). Ozean und Antarktis meereokundliche Forschungen und Ergebnisse der Deutschen Sudpolar Expedition, 1901-03. *De Gruyter*, *7*(5), 387–556.

Wadley, M., & Bigg, G. (1995). Abyssal channel flow in ocean circulation models with application to the Vema Channel. *Journal of Physical Oceanography*, *26*(1), 38–48. https://doi.org/10.1175/1520-0485(1996)026<0038:acfiog>2.0.co;2

Warren, B. A., & Speer, K. G. (1991). Deep circulation in the eastern South Atlantic Ocean. *Deep-Sea Research Part* I, *3*8, 281–322. https://doi.org/10.1016/S0198-0149(12)80014-8

Whitehead, J. A. (1989). Giant ocean cataracts. *Scientific America*n, *26*0(2), 50–57. https://doi.org/10.1038/scientificamerican0289-50

Whitehead, J. A. (1998). Topographic control of oceanic flows in deep passages and straits. *Review of Geophysics*, *36*(3), 423–440. https://doi.org/10.1029/98RG01014

Whitehead, J. A., Leetma, A., & Knox, R. A. (1974). Rotating hydraulics of strait and sill flows. *Geophysical Fluid Dynamics*, *6*(2), 101–125. https://doi.org/10.1080/03091927409365790

Whitehead, J. A., & Worthington, L. V. (1982). The flux and mixing rates of Antarctic Bottom Water within the North Atlantic. *Journal of Geophysical Research*, *87*(C10), 7903–7924. https://doi.org/10.1029/jc087ic10p07903

Wright, W. R. (1970). Northward transport of Antarctic Bottom Water in the Western Atlantic Ocean. *Deep-Sea Research Part I*, *17*(2), 367–371. https://doi.org/10.1016/0011-7471(70)90028-8

Wüst, G. (1936). Schichtung und Zirkulation des Atlantischen Ozeans. In A. Defant (Ed.), *Wissenschaftliche Ergebnisse, Deutsche Atlantische Expedition auf dem Forschungs—und Vermessungsschiff "Meteor" 1925–1927* (Vol. 6). Walter de Gruyter & Co.

Xiong, L., Tang, G., Yang, X., & Li, F. (2021). Geomorphology-oriented digital terrain analysis: Progress and perspectives. *Journal of Geographical Sciences*, *31*(3), 456–476. https://doi.org/10.1007/s11442-021-1853-9